ARL13B regulates Sonic Hedgehog signaling from outside primary cilia

Eduardo D. Gigante[a,b], Megan R. Taylor[c], Anna A. Ivanova[d], Richard A. Kahn[d], Tamara Caspary[b]

[a]Neuroscience Graduate Program, [b]Department of Human Genetics, [c]Emory College of Arts and Sciences, [d]Department of Biochemistry, Emory University School of Medicine, Atlanta, GA 30322, USA

Author e-mails: Eduardo.gigante@emory.edu, meg96taylor@gmail.com, anna.ivanova@emory.edu, rkahn@emory.edu

ORCID ID: Gigante: 0000-0002-1486-5377, Kahn: 0000-0002-0259-0601, Caspary: 0000-0002-6579-7589

⌘**Correspondence**: Tamara Caspary

tcaspar@emory.edu

Abstract

ARL13B is a regulatory GTPase highly enriched in cilia. Complete loss of *Arl13b* disrupts cilia architecture, protein trafficking and Sonic hedgehog signaling. To determine whether ARL13B is required within cilia, we knocked in a cilia-excluded variant of ARL13B (V358A) and showed it retains all known biochemical function. We found that ARL13B^{V358A} protein was expressed but could not be detected in cilia, even when retrograde ciliary transport was blocked. We showed *Arl13b*$^{V358A/V358A}$ mice are viable and fertile with normal Shh signal transduction. However, in contrast to wild type cilia, *Arl13b*$^{V358A/V358A}$ cells displayed short cilia and lacked ciliary ARL3 and INPP5E. These data indicate that ARL13B's role within cilia can be uncoupled from its function outside of cilia. Furthermore, these data imply that the cilia defects upon complete absence of ARL13B do not underlie the alterations in Shh transduction, which is unexpected given the requirement of cilia for Shh transduction.

Keywords:

ARL13B; Sonic Hedgehog signaling; primary cilia; mouse development

Introduction

The Hedgehog (Hh) signaling pathway is essential for embryogenesis in a wide variety of organisms. Initially discovered in *Drosophila* where there is a single Hh ligand, the core components of the Hh pathway are conserved in vertebrates (Nusslein-Volhard et al. 1980). These include the vertebrate Hh receptor Patched1 (Ptch1), the obligate transducer of the pathway Smoothened (Smo), as well as the Gli transcription factors (Ci in *Drosophila*) that act as both activators (GliA) and repressors (GliR) to control target gene transcription (Briscoe et al. 2013). There are three Hh ligands in vertebrates, Sonic (Shh), Indian (Ihh) and Desert (Dhh), that regulate a multitude of developmental processes including formation of the limbs and digits, the bones of the skull and face, and the patterning of the neural tube (Placzek et al. 2018). Diminished Hh signaling during embryogenesis results in birth defects whereas increased Hh signaling leads to tumors, highlighting the importance of the pathway and its regulation (Raleigh et al. 2019).

Given the deep homology between invertebrate and vertebrate Hh signaling, the discovery that primary cilia are required for vertebrate, but not invertebrate, Hh signaling was unexpected (Huangfu et al. 2003; Huangfu et al. 2006). Vertebrate Hh components dynamically traffic within primary cilia in response to Hh ligand (Corbit et al. 2005; Haycraft et al. 2005; Rohatgi et al. 2007). In the absence of ligand, Ptch1 is enriched on the ciliary membrane and Smo is barely detectable (Corbit et al. 2005; Rohatgi et al. 2007). Furthermore, full length Gli proteins traffic to the ciliary tip and back to the cytoplasm before being cleaved to their repressor form, which actively shuts down Hh target gene transcription in the nucleus (Kim et al. 2009; Liu et al. 2005; Wen et al.

2010; Humke et al. 2010). In contrast, upon ligand stimulation (Shh, Ihh or Dhh), the Ptch1 receptor binds the ligand and shuttles out of cilia (Rohatgi et al. 2007). Subsequently, Smo is enriched in the cilium and is subsequently activated (Kong et al. 2019; Corbit et al. 2005). Activated Smo promotes the processing of full-length Gli transcription factors into GliA, which turns on target genes (Aza-Blanc et al. 2000; Ruiz i Altaba 1998). Ablation of cilia results in an absence of GliA and GliR production, rendering the pathway inert and leading to an absence of transcriptional response (Huangfu et al. 2005). The dynamic ciliary movement of Shh components appears to be critical to pathway function, as alterations to cilia disrupt pathway output (Caspary et al. 2007; Huangfu et al. 2006; Liem et al. 2012; Liem et al. 2009; Goetz et al. 2009; Murdoch et al. 2010; Tuz et al. 2014; Cortellino et al. 2009; Houde et al. 2006; Liu et al. 2005; Tran et al. 2008; Taylor et al. 2015).

Given that the fundamental logic of the pathway is conserved from flies through vertebrates, and that flies transduce Hh signals without relying on primary cilia, both evolutionary and mechanistic questions are raised as to how vertebrate cells co-opted the primary cilium for Hh signal transduction. One distinction lies in the fact that vertebrates use Hh signaling over a longer distance than flies, leading to the proposal that the primary cilium is a critical part of a mechanism underlying long range signaling (Bangs et al. 2015). For example, in neural patterning Shh is initially expressed in the notochord and is secreted to specify fates more than 20 cells away (Chiang et al. 1996; Briscoe et al. 2001; Roelink et al. 1994). At the evolutionary level, comparisons among organisms with cilia and or Hh have provided some clues. The round worm *C. elegans* have cilia yet do not possess Hh signaling as they don't have most of the genes

encoding the core components of Hh signal transduction (Consortium 1998; Roy 2012). Curiously, a few components of Hh signaling such as fused and costal 2 are in the *C. elegans* genome where they are functionally important for ciliogenesis (Ingham et al. 2011). Additionally, *C. elegans* retained a Ptch1 homolog important for development and pattern formation, but no Hh or Smo (Zugasti et al. 2005; Kuwabara et al. 2000). In contrast, planaria flatworms possess both cilia and Hh signaling but the cilia are not required to transduce Hh signaling (Rink et al. 2009). The first known evolutionary link between cilia and Hh is in sea urchins which transduce Hh signal in developing muscle tissue via motile cilia (Warner et al. 2014; Sigg et al. 2017). Subsequently, in vertebrates Hh signaling requires primary cilia. These data suggest that the mechanistic link of cilia and Hh is limited to deuterostomes and raises the question of whether the relationship of Hh and primary cilia originated near the last common ancestor of vertebrates, the urochordates.

ARL13B is a member of the ARF family of regulatory GTPases and is highly enriched on the ciliary membrane (Caspary et al. 2007). In mice, a null mutation of *Arl13b* leads to short cilia and to alterations in Shh signal transduction (Caspary et al. 2007; Larkins et al. 2011). ARL13 is ancient, predicted to be present in the last common eukaryotic ancestor. ARL13 appears to have been lost during evolution in organisms that lack cilia and duplicated to ARL13A and ARL13B in the urochordates, thus ARL13B is proposed to hold important clues in deciphering the links between primary cilia and vertebrate Hh signaling (Schlacht et al. 2013; Li et al. 2004; Kahn et al. 2008; East et al. 2012; Logsdon et al. 2004).

ARF regulatory GTPases, like ARL13B, are best known to play roles in membrane trafficking (D'Souza-Schorey et al. 2006). As is true for a large number of regulatory GTPases, ARL13B is functionally diverse (Sztul et al. 2019). It regulates endocytic traffic (Barral et al. 2012), as well as the phospholipid composition of the ciliary membrane through recruitment of the lipid phosphatase INPP5E to the ciliary membrane (Humbert et al. 2012). ARL13B also has a conserved role as a guanine nucleotide exchange factor (GEF) for ARL3, another ciliary ARF-like (ARL) protein (Gotthardt et al. 2015; Zhang et al. 2016; Hanke-Gogokhia et al. 2016; Ivanova et al. 2017). ARL13B regulates intraflagellar transport (IFT), the process that builds and maintains cilia (Cevik et al. 2010; Li et al. 2010; Nozaki et al. 2017). It is known to interact with several proteins associated with cilia, including the exocyst, tubulin and UNC119 (Seixas et al. 2016; Zhang et al. 2016; Larkins et al. 2011; Revenkova et al. 2018). Critical to this work, loss of ARL13B disrupts Shh signal transduction in at least two distinct ways: Smo enrichment in cilia occurs even in the absence of ligand and Gli activator production is diminished, although Gli repressor is made normally (Caspary et al. 2007; Larkins et al. 2011).

Due to the high enrichment of ARL13B on the ciliary membrane, ARL13B is assumed to function in its diverse roles from within the cilium. However, ARL13B is present in early endosomes and circular dorsal ruffles on the cell surface (Barral et al. 2012; Casalou et al. 2014). We previously showed that a V358A variant of ARL13B does not localize to cilia as it disrupts a known VxPx cilia localization sequence (Higginbotham et al. 2012; Mariani et al. 2016). Exogenous overexpression of a ARL13B^{V358A} construct in *Arl13b* null cells does not rescue ARL13B-dependent

phenotypes such as cilia length as well as interneuron migration and connectivity, consistent with ciliary ARL13B mediating these processes (Higginbotham et al. 2012; Mariani et al. 2016). In contrast, we found that overexpressed ARL13B^{V358A} does rescue the Shh-dependent ciliary enrichment of Smo in mouse embryonic fibroblasts, arguing that ARL13B may function outside the cilium to regulate Smo traffic (Mariani et al. 2016). Together, these results raise the question of where ARL13B functions.

To define where ARL13B functions in relation to cilia, we wanted an *in vivo* model so generated mice carrying the ARL13B^{V358A} point mutation using CRISPR/Cas9. Here we demonstrate that ARL13B^{V358A} protein was undetectable in *Arl13b$^{V358A/V358A}$* cilia in both neural tube and mouse embryonic fibroblast cilia, even after blocking retrograde ciliary traffic. We report that *Arl13b$^{V358A/V358A}$* mice were viable, fertile, and transduced Shh signal normally. We found ARL3 and INPP5E did not localize to the short cilia present in/on *Arl13b$^{V358A/V358A}$* cells. These data indicate that ARL13B's roles within and outside cilia can be uncoupled; ARL13B's role in regulating cilia length is from within cilia, whereas its control of Shh signaling appears to be from outside the cilium. Thus, these data imply that the cilia defects seen in the complete absence of ARL13B do not underlie the alterations in Shh transduction, which is unexpected given the requirement of cilia for Shh signal transduction.

Results

ARL13B^{V358A} *displays normal GEF activity*

We previously showed that mouse ARL13B^{V358A} protein retained normal intrinsic and GAP-stimulated GTP hydrolysis activities by analyzing GST-ARL13B^{V358A} purified

from human embryonic kidney (HEK) cells (Mariani et al. 2016). In order to test ARL13B^{V358A} GEF activity for ARL3, we used the same GST-ARL13B^{V358A} protein preparation and measured the rates of spontaneous or GEF-stimulated GDP dissociation from ARL3 in the presence and absence of ARL13B or ARL13B^{V358A}. ARL3 spontaneously releases pre-bound GDP quite slowly under the conditions in the assay, though release is linear with time, and by extrapolation requires just under 30 min for 50% of pre-bound [^{3}H]GDP to dissociate (**Figure 1**). In marked contrast, addition of ARL13B under the same conditions caused the release of 50% of the GDP within ~10 seconds and close to 100% in one minute. We detected no differences between the wild type and mutant ARL13B^{V358A} proteins in this assay, consistent with this point mutation having no effect on ARL13B GEF function (**Figure 1**). This result is consistent with GEF activity being conserved within the protein's GTPase domain while the V358A mutation is located in the C-terminal domain (Gotthardt et al. 2015). These data indicate that ARL13B^{V358A} retains all known ARL13B biochemical activities, suggesting that the V358A mutation only disrupts ARL13B localization.

CRISPR engineered* Arl13b$^{V358A/V358A}$ *mice express cilia-excluded ARL13B protein.

To determine the consequences of ARL13B^{V358A} expression *in vivo*, we used CRISPR/Cas9 editing to change residue 358 from valine to alanine (**Figure 2A**). We performed sequencing of the region that flanked exon 8, using primers outside the region of the donor oligonucleotide. We confirmed the heterozygous T to C base pair change for a valine to alanine change at residue 358 (**Figure 2B**). We backcrossed

heterozygous F1 progeny to FVB/NJ for three generations before analysis to minimize any off target confounds (see details in Methods).

To determine whether ARL13B^{V358A} was detectable in neural tube cilia, we performed immunofluorescence using antibodies directed against ARL13B and the cilia marker IFT88. At embryonic day (E)10.5, we saw IFT88 staining, indicating the presence of cilia. In neural tube cilia of *Arl13b*$^{+/+}$ and *Arl13b*$^{V358A/+}$ embryos, we observed equivalent ARL13B staining but could not see ARL13B signal in neural tube cilia of *Arl13b*$^{V358A/V358A}$ embryos (**Figure 2C**). We exposed the images longer, to saturation, and while we observed low-level staining throughout the cell, we saw no ciliary ARL13B indicating the ARL13B^{V358A} protein is undetectable in cilia *in vivo* (**Figure 2 – Figure supplement 1**).

One possible explanation for the absence of ciliary ARL13B in the *Arl13b*$^{V358A/V358A}$ embryos is that the ARL13B^{V358A} protein is not expressed or is unstable. To determine whether ARL13B protein expression was affected by the V358A mutation, we performed Western blots on E10.5 whole embryo lysates (**Figure 2D**). We found a ~7% (±20%) reduction of ARL13B levels in *Arl13b*$^{V358A/+}$ embryos and a ~37% (±6%) decrease of ARL13B levels in *Arl13b*$^{V358A/V358A}$ embryos, compared to WT (**Figure 2E**). This decrease may reflect a change in ARL13B^{V358A} stability compared to ciliary ARL13B or could signify ARL13B^{V358A} protein having a distinct half-life when localizing to different cellular compartments. Regardless, these data indicate that ARL13B^{V358A} is expressed in *Arl13b*$^{V358A/V358A}$ embryos.

ARL13B^{V358A} protein is undetectable in cilia in mouse embryonic fibroblasts.

To more closely investigate whether any ARL13B^{V358A} protein could localize to cilia, we generated immortalized mouse embryonic fibroblasts (MEFs). We performed double labeling to first identify cilia using acetylated α-tubulin or IFT88 antibodies and subsequently determined whether ARL13B is present in cilia. We used five distinct antibodies against ARL13B: 4 antibodies against amino acids 208-427 of the mouse ARL13B protein (1 mouse monoclonal (NeuroMab), 3 rabbit polyclonal antibodies (Caspary et al. 2007)), as well as 1 antibody against the full-length human ARL13B protein (rabbit polyclonal (Protein Tech)). By eye, we observed strong ciliary staining of ARL13B with each of the antibodies in *Arl13b*$^{+/+}$ and *Arl13b*$^{V358A/+}$ cells, but we were unable to identify any evidence of ARL13B staining above background within cilia in *Arl13b*$^{V358A/V358A}$ cells with any of these five antibodies (**Figure 3A**). Taken together, these data support our conclusion that ARL13B^{V358A} is not detectable in cilia using the currently available, validated ARL13B antibodies. While we observed no evidence of detectable ciliary ARL13B in *Arl13b*$^{V358A/V358A}$ MEFs, it is possible that a small amount of ARL13B^{V358A} is constantly trafficking in and out of cilia, at steady-state levels that remain below the limits of detection. To begin to address this possibility, we blocked retrograde ciliary transport, reasoning that any ARL13B undergoing trafficking in and out of cilia would accumulate. We treated cells with ciliobrevin-D, which blocks the retrograde motor protein dynein (Firestone et al. 2012). As a positive control, we examined IFT88 and Gli3, a ciliary protein and a Hh component, respectively; both are known to accumulate at ciliary tips upon blocking of retrograde transport. We found IFT88 and Gli3 enrichment at ciliary tips in *Arl13b*$^{+/+}$, *Arl13b*$^{V358A/+}$ and *Arl13b*$^{V358A/V358A}$

cells upon ciliobrevin-D treatment relative to the respective DMSO-treated controls with no difference in IFT88 or Gli3 staining among the 3 genotypes (**Figure 3B and C**). To determine whether ARL13B accumulated in cilia of ciliobrevin-D-treated MEFs, we examined cells co-stained for acetylated α-tubulin and ARL13B. In *Arl13b*$^{+/+}$ and *Arl13b*$^{V358A/+}$ cells, we saw that about 90% of acetylated α-tubulin-positive cilia also stained for ARL13B in DMSO-treated control or ciliobrevin-D treated MEFs (**Figure 3D and E**). In *Arl13b*$^{V358A/V358A}$ MEFs, we saw no ciliary ARL13B staining in DMSO-treated control or ciliobrevin-D-treated cells using 2 antibodies against distinct epitopes (**Figure 3D and E)**. Thus, even when retrograde traffic out of cilia is disrupted, we were unable to detect ARL13B protein in cilia in *Arl13b*$^{V358A/V358A}$ MEFs.

We re-examined these data and repeated our analyses using over-exposed images. After defining the region of interest using the acetylated α-tubulin staining, we subsequently overexposed the ARL13B channel five-fold relative to the images in Figure 3 and acquired measurements at the cilium and the cell body (**Figure 3 – Figure supplement 1**). As a control, we used *Arl13b*$^{hnn/hnn}$ MEFs, which are devoid of any ARL13B, and obtained a ratio of 1.0, with or without ciliobrevin-D treatment. We found the same ratio when we analyzed *Arl13b*$^{V358A/V358A}$ MEFs consistent with ARL13B being absent from the cilia. We observed a few instances of ARL13B appearing to co-localize with acetylated α-tubulin, but these were rare (<5%, 2/49) and occurred in both *Arl13b*$^{V358A/V358A}$ and *Arl13b*$^{hnn/hnn}$ (null) cells indicating this is the background staining of the primary antibody. We extended our analysis of overexposed images in *Arl13b*$^{V358A/V358A}$ and *Arl13b*$^{hnn/hnn}$ neural tube sections four-fold relative to the images in Figure 2; we identified no overlap of overexposed ARL13B with cilia marker IFT88

(**Figure 2 – Figure supplement 1**). While it is formally possible that an extremely small amount of ARL13B^{V358A} remains in cilia, we are not able to find evidence of it; thus, we designate ARL13B^{V358A} protein as cilia-excluded ARL13B.

We did not observe any obvious cellular ARL13B signal in the cells expressing cilia-excluded ARL13B so we investigated whether we could detect cellular ARL13B in cells lacking cilia, *IFT172^{wim}* MEFs. As controls we used wildtype, *Arl13b^{hnn}* (lacking ARL13B), and *IFT172^{wim} Arl13b^{hnn}* (lacking ARL13B and cilia) MEFs. We only detected ARL13B staining in *IFT172^{wim}* cells upon overexposure and found it was modestly detectable above the background level we observed in *Arl13b^{hnn}* or *IFT172^{wim} Arl13b^{hnn}* cells (**Figure 3 – Figure supplement 2**). Thus, cellular ARL13B is expressed at an extremely low level.

Arl13b$^{V358A/V358A}$ mice are viable and fertile.

In order to determine the phenotypic consequence of the *Arl13b^{V358A}* allele, we intercrossed *Arl13b$^{V358A/+}$* mice. We observed progeny in Mendelian proportions with an average of 7.3 pups per litter, consistent with the reported FVB/NJ litter size of 7-9 (Murray et al. 2010) (**Table 1**). To test whether homozygous mice breed normally, we crossed *Arl13b$^{V358A/V358A}$* males to heterozygous or homozygous females. We found the *Arl13b^{V358A}* allele segregated in Mendelian proportions and the litter sizes were normal indicating that *Arl13b^{V358A}* does not impact viability, fertility or fecundity.

237 ***ARL13B^{V358A} permits normal embryonic development and Shh signaling.***

238 Loss of *Arl13b* leads to morphologically abnormal embryos, lethality and neural
239 patterning defects (Caspary et al. 2007). As ARL13B^{V358A} overcame the embryonic
240 lethality, we examined overall embryo morphology at E9.5, E10.5 and E12.5. We found
241 the overall morphology of *Arl13b$^{V358A/V358A}$* embryos resembled those of *Arl13b$^{+/+}$* and
242 *Arl13b$^{V358A/+}$* embryos indicating that ARL13B^{V358A} did not lead to gross morphological
243 defects. (**Figure 4A-I**).

244 At E9.5, Shh is normally expressed in the notochord as well as the floor plate of
245 the ventral neural tube. Moving dorsally, the adjacent domains express Nkx2.2 and
246 subsequently Olig2. In the *Arl13b$^{hnn/hnn}$* (null) neural tube, the Shh-positive columnar
247 cells of the floor plate are absent resulting in both ventral and dorsal expansion of
248 intermediate Shh-dependent cell fates such as Olig2 (Caspary et al. 2007). To
249 determine whether ARL13B^{V358A} disrupts Shh signaling, we examined neural tube
250 patterning in *Arl13b$^{+/+}$*, *Arl13b$^{V358A/+}$*, and *Arl13b$^{V358A/V358A}$* embryos at E9.5, E10.5, and
251 E12.5. At E9.5 we observed no differences in Shh, Nkx2.2 or Olig2 among *Arl13b$^{+/+}$*,
252 *Arl13b$^{V358A/+}$*, and *Arl13b$^{V358A/V358A}$* embryos (**Figure 4A-C**). Cell fates in the neural tube
253 are specified by both the concentration and duration of Shh signaling so we examined
254 neural patterning at subsequent stages (Dessaud et al. 2007). By E10.5, some Olig2
255 precursors have differentiated to HB9+ motor neurons and all Shh-responsive cells
256 express Nkx6.1. We found that Olig2, HB9 and Nkx6.1 positive cells are normally
257 distributed in all 3 genotypes at E10.5 and E12.5 (**Figure 4D-I**). These data indicate that
258 ARL13B^{V358A} mediates normal Shh signaling.
259

ARL13B regulates ciliary enrichment of Shh components from outside cilia.

In *Arl13b*$^{hnn/hnn}$ cells, Smo is enriched in cilia in a Shh-independent manner, which may be due to defective trafficking of Smo, as many ARL family members regulate protein trafficking (Lim et al. 2011; Larkins et al. 2011). To assess Smo enrichment in *Arl13b*$^{V358A/V358A}$ embryos, we stained for the cilia marker acetylated α-tubulin and Smo in E10.5 embryos. Smo appeared enriched normally in ventral floor plate cilia and the dorsal boundary of Smo ciliary enrichment in ventral neural progenitors was identical in *Arl13b*$^{+/+}$, *Arl13b*$^{V358A/+}$, and *Arl13b*$^{V358A/V358A}$ samples indicating ARL13B^{V358A} mediates normal ciliary Smo enrichment (**Figure 5A)**.

To examine Smo traffic in response to Shh stimulation, we treated MEFs with 0.5% FBS or Shh-conditioned media for 24 hours and stained for Smo. As expected in control *Arl13b*$^{hnn/hnn}$ cells, we saw ciliary Smo in unstimulated MEFs which increased upon stimulation with Shh-conditioned media (Larkins et al. 2011) (**Figure 5B**). In *Arl13b*$^{+/+}$, *Arl13b*$^{V358A/+}$, and *Arl13b*$^{V358A/V358A}$ MEF cilia, we saw ciliary enrichment of Smo upon Shh stimulation over their respective unstimulated controls (**Figure 5B**, left). We found no difference in Smo enrichment among these cell lines (**Figure 5B**, right). Thus, despite ARL13B being critical for Shh-dependent Smo ciliary enrichment, ARL13B^{V358A} regulates Smo localization normally, arguing this function of ARL13B can occur when the protein is not in cilia.

In addition to aberrations in Smo trafficking, loss of *Arl13b* leads to changes in the cilia localization of other Shh components in MEFs (Larkins et al. 2011). To determine whether these components are disrupted by ARL13B^{V358A}, we examined Gli2, Gli3, Sufu and Ptch1 in MEFs. We observed no differences in distribution of Gli2 or

283 Ptch1 among any of the examined genotypes (**Figure 5C, F**). In contrast, as we
284 previously reported, we observed more Gli3 at the ciliary tip of *Arl13b*$^{hnn/hnn}$ cells and
285 increased Sufu in *Arl13b*$^{hnn/hnn}$ cilia compared to wild type controls (Larkins et al.
286 2011)(**Figure 5D, E**). Thus, Shh components are normally localized in *Arl13b*$^{V358A/V358A}$
287 MEFs consistent with the normal Shh signal transduction observed in *Arl13b*$^{V358A/V358A}$
288 embryos (**Figure 4**).
289
290 ***ARL13B regulates ciliary enrichment of ARL3 and INPP5E from within cilia.***
291 We next examined the role of ARL13B^{V358A} in the localization of other ciliary
292 proteins. ARL13B is the GEF for ARL3, and we showed that ARL13B^{V358A} GEF activity
293 for ARL3 is retained (**Figure 1**). ARL13B is also essential for cilia localization of
294 INPP5E, as the proteins are in a common complex (Humbert et al. 2012). To determine
295 whether the ciliary localization of either ARL3 or INPP5E was affected by ARL13B^{V358A},
296 we performed immunofluorescence on MEFs. Ciliary ARL3 staining appeared the same
297 in *Arl13b*$^{+/+}$ and *Arl13b*$^{V358A/+}$ MEFs, however ARL3 was not detectable in
298 *Arl13b*$^{V358A/V358A}$ or *Arl13b*$^{hnn/hnn}$ cilia (**Figure 5G**). INPP5E was normally detectable in
299 *Arl13b*$^{+/+}$ and *Arl13b*$^{V358A/+}$ MEF cilia, but not in *Arl13b*$^{V358A/V358A}$ and *Arl13b*$^{hnn/hnn}$ MEF
300 cilia (**Figure 5H**). These results indicate that ARL13B is required in cilia for the proper
301 localization of ARL3 and INPP5E to the cilium.
302
303 ***Ciliary ARL13B is required for normal cell ciliation and ciliary length***
304 Loss of *Arl13b* leads to defects in the percentage of ciliated MEFs and in cilia
305 length (Caspary et al. 2007; Larkins et al. 2011). To test whether ARL13B^{V358A} impacted

306 cell ciliation, we examined immortalized MEFs and counted the number of ciliated cells
307 24 hours after induction of ciliation by growth in low serum (0.5% FBS). We found 73%
308 (±11%) of *Arl13b*$^{+/+}$ and 75%, (±9.1%) of *Arl13b*$^{V358A/+}$ MEFs are ciliated, consistent with
309 published results. In contrast, we found 45% (±8.7%) of *Arl13b*$^{V358A/V358A}$ cells and 53%
310 (±6.4%) of *Arl13b*$^{hnn/hnn}$ cells had cilia (**Figure 6A**). Thus, *Arl13b*$^{V358A/V358A}$ cells exhibit a
311 similar deficit in percentage of ciliated MEFs as complete loss of ARL13B function.
312 *Arl13b*$^{hnn/hnn}$ cilia are about half as long as wild type in both embryos and MEFs
313 (Caspary et al. 2007; Larkins et al. 2011). To determine whether cilia length was
314 affected by ARL13B^{V358A}, we stained MEFs with acetylated α–tubulin and measured the
315 length of the axoneme. We found the average cilia length in *Arl13b*$^{+/+}$ and Arl13b$^{V358A/+}$
316 MEFs was similar, 2.7 ± 0.8 μm and 2.6 ± 0.9 μm, respectively. However, we found
317 *Arl13b*$^{V358A/V358A}$ MEF cilia were shorter, 1.9 ± 0.7 μm, similar to *Arl13b*$^{hnn/hnn}$ MEF cilia
318 which were 2.15 ± 0.8 μm (**Figure 6B**). These results indicate that ARL13B^{V358A}
319 phenocopies complete loss of ARL13B for ciliation and cilia length, indicating these
320 ARL13B functions require ARL13B in cilia. Furthermore, these data show that ARL13B
321 function within cilia is distinct from ARL13B function outside of cilia in a subset of
322 activities, and that the cilia defects and Shh defects in the complete absence of ARL13B
323 can be uncoupled.

Discussion

324 Here we show that ARL13B's role(s) in cell ciliation and cilia length, along with
325 the ciliary enrichment of a subset of proteins, can be uncoupled from ARL13B's function
326 in regulating Shh signal transduction (**Figure 7**). Furthermore, we show this functional

distinction correlates with ARL13B spatial localization to the cilium. By generating a mouse expressing a cilia-excluded variant of ARL13B from the endogenous locus, we showed ARL13B^{V358A} protein is not detectable in cilia of embryonic neural tube or MEFs, even upon retrograde ciliary dynein traffic blockade. Furthermore, we detected 30% less ARL13B protein overall in *Arl13b*$^{V358A/V358A}$ embryos compared to control embryos. While this reduction is statistically significant, it is unclear whether it is biologically significant given that *Arl13b*$^{hnn/hnn}$ null mutations are recessive and no *Arl13b*$^{hnn/+}$ heterozygous phenotype is reported (Caspary et al. 2007; Larkins et al. 2011).

In contrast to the E13.5 lethality of *Arl13b*$^{hnn/hnn}$ embryos, we found *Arl13b*$^{V358A/V358A}$ mice were viable and fertile with correct patterning of the neural tube, indicating normal Shh signal transduction. These results are consistent with our data showing that ARL13B^{V358A} protein retains all known biochemical function including GEF activity (Mariani et al. 2016; Ivanova et al. 2017). However, we observed several *Arl13b*$^{hnn/hnn}$ phenotypes in *Arl13b*$^{V358A/V358A}$ cells, including loss of ARL3 and INPP5E ciliary enrichment, along with low percentage of ciliated cells and shorter average cilia length. Taken together, our data show that despite the normal high ciliary enrichment of wild type ARL13B and the requirement of cilia for Shh signaling, cilia-excluded ARL13B^{V358A} is sufficient for Shh signal transduction.

We regard ARL13B^{V358A} as cilia-excluded based on several lines of evidence. We did not detect ciliary ARL13B^{V358A} *in vivo* or *in vitro* using any of five validated ARL13B antibodies. These antibodies are against two antigens, the full-length protein or residues 208-427, and were independently generated so are likely to recognize a

number of epitopes. Given that 4 of 5 antibodies are polyclonal and ARL13B^{V358A} displays normal GTP binding, intrinsic and GAP-stimulated GTP hydrolysis, and ARL3 GEF activity, it is likely that the ARL13B^{V358A} protein retains the wild type structure enabling antibody recognition. Indeed, we observed little or no loss in sensitivity in detecting protein in the immunoblot assays. Furthermore, we could not forcibly enrich ciliary ARL13B^{V358A} through retrograde transport blockade with ciliobrevin-D nor could we detect any ciliary enrichment of ARL13B^{V358A} upon overexposure of the relevant fluorescent channel. Alternative ways of trafficking proteins out of cilia include BBSome-dependent or diffusion-dependent mechanisms raising the possibility that ARL13B is not trafficked via dynein-independent mechanisms. The fact that we observed ciliary phenotypes, namely short cilia and abnormal ciliary ARL3 and INPP5E localization in ARL13B^{V358A} cells, argue that ARL13B normally performs these functions from within cilia (Caspary et al. 2007; Larkins et al. 2011; Zhang et al. 2016; Humbert et al. 2012; Nozaki et al. 2017). While we cannot exclude the possibility that sub-detectable levels of ARL13B^{V358A} are present and functional in cilia, we note such a level would need to be sufficient for Shh signaling yet insufficient for ARL3 or INPP5E ciliary localization along with proper regulation of cilia length.

Our data support ARL13B regulating different biological processes from its distinct subcellular localizations. ARL13B^{V358A} disrupts cilia localization of INPP5E and ARL3, but not Shh components. It is surprising that ARL13B^{V358A} is sufficient to regulate Shh signaling because cilia are required for Shh signal transduction and because ARL13B is highly enriched in cilia (Caspary et al. 2007; Huangfu et al. 2003). These observations suggested that the ciliary defects observed in *Arl13b*$^{hnn/hnn}$ mutants caused

373 the Shh defects. However, our data with ARL13B^{V358A} indicate that ARL13B regulates
374 cilia length and Shh signaling through distinct localization and effectors. Thus, the cilia
375 defects in *Arl13b$^{hnn/hnn}$* mutants do not underlie Shh misregulation.
376 Based on the normal cilia trafficking of Shh components in *Arl13b$^{V358A/V358A}$*
377 mutants and the abnormal cilia trafficking of Shh components in the complete absence
378 of ARL13B (Larkins et al. 2011), ARL13B likely regulates Shh signaling from the cell
379 body by controlling Shh component traffic to and/or from the primary cilium. Both Smo
380 and ARL13B traffic is linked to endosomes providing one possible non-ciliary organelle
381 (Barral et al. 2012; Wang et al. 2009; Milenkovic et al. 2009). *Arl13b$^{hnn/hnn}$* cells display
382 constitutive Smo ciliary enrichment along with little enrichment of Gli proteins at the
383 ciliary tip (Larkins et al. 2011). Our data do not distinguish between ARL13B playing
384 direct roles in traffic of multiple Shh components or whether the normal Smo ciliary
385 enrichment with ARL13B^{V358A} subsequently causes normal cilia traffic of downstream
386 components. ARL13B regulates a step downstream of activated Smo that controls
387 transcription factor Gli activation, but not repression (Caspary et al. 2007; Bay et al.
388 2018). We argue from our results that this step is also intact in the presence of
389 ARL13B^{V358A}.
390 The fact that ARL13B^{V358A} can mediate normal ciliary Smo enrichment is
391 especially interesting given that ARL3 and INPP5E localization to cilia is compromised
392 by this mutation. This suggests that ARL13B controls cilia enrichment via multiple
393 localizations and effectors. This is consistent with our understanding of ARF family
394 members, as they are known to perform multiple tasks from different sites within a cell
395 (Sztul et al. 2019). We speculate that ARL3 residence in cilia may require that ARL3 be

in (or at least cycle through) its activated, GTP-bound conformation as ARL13B^{V358A} retains its ARL3 GEF activity, but not its cilia localization. ARL13B is in a common protein complex with INPP5E so absence of ARL13B from cilia may disrupt formation or maintenance of the complex there (Humbert et al. 2012; Nozaki et al. 2017). INPP5E regulates Shh signaling through regulation of the phosphoinositol composition of the ciliary membrane. INPP5E loss results in increased ciliary PIP_2 and enrichment of Shh repressors in cilia thus resulting in lowered Shh response (Garcia-Gonzalo et al. 2015; Chavez et al. 2015; Dyson et al. 2017). It is not clear why the absence of ciliary INPP5E in ARL13B^{V358A} cells does not lead to aberrant Shh signal transduction.

In *Arl13b$^{hnn/hnn}$* embryos and MEFs, cilia are shorter than normal and have a microtubule defect where the B-tubule of the microtubule outer doublet is open (Caspary et al. 2007; Larkins et al. 2011). Consistent with this, we observed shorter cilia in *Arl13b$^{V358A/V358A}$* MEFs. Similarly, we observed a comparable reduction in the percent of cilia in *Arl13b$^{hnn/hnn}$* and *Arl13b$^{V358A/V358A}$* MEFs compared to wild type MEFs. While loss of ARL13B results in short cilia, increased expression of ARL13B promotes cilia elongation so it is not yet clear what ARL13B's role is in controlling cilia length (Lu et al. 2015; Hori et al. 2008; Caspary et al. 2007; Larkins et al. 2011). Additionally, it is unclear whether the mechanism from within cilia through which ARL13B controls length or percent of ciliated cells is the same, or distinct from, the mechanism through which ARL13B regulates ARL3 or INPP5E residence in cilia.

Perhaps the most intriguing implication of our data pertains to understanding the evolution of cilia and Hh signaling. ARL13 functions in cilia formation and maintenance in *Chlamydomonas* and *C. elegans*, neither of which have Hh signaling, consistent with

419 the ancient role of ARL13 controlling ciliation and cilia length (Cevik et al. 2010; Cevik et
420 al. 2013; Stolc et al. 2005; Miertzschke et al. 2014). Our data support ARL13B retaining
421 ARL13's ancient role in ciliogenesis. However, our data show that ARL13B does not
422 work from within the cilium to regulate Shh component ciliary traffic or Shh signal
423 transduction. As an ARL protein involved in membrane traffic, we speculate that
424 ARL13B may have linked Shh component trafficking to the primary cilium, albeit from
425 outside the cilium. That the ARL13 duplication could relate to the mechanism linking
426 primary cilia and Hh signaling within the deuterostome lineage is a possibility worth
427 exploring.
428

Key Resources Table

Reagent type (species) or resource	Designation	Source or reference	Identifiers	Additional information
gene (*M. Musculus*)	*Arl13b*		MGI Cat# 6115585, RRID:MGI:6115585	
Genetic reagent (*M. Musculus)*	*hennin*	PMID:17488627	MGI Cat# 3580673, RRID:MGI:3580673	*Arl13b* null allele
Genetic reagent (*M. Musculus)*	*em1Tc* (*V358A*)	This paper	MGI: 6256969	New CRISPR Point mutant
Genetic reagent (*M. Musculus)*	FBV/NJ	Jackson Laboratory	Stock #001800 MGI:2163709	
cell lines (*M. Musculus*)	Fibroblast (normal, embryonic)	This paper		Maintained in Caspary lab

Antibody	Anti-Shh (Mouse Monoclonal)	Developmental Studies Hybridoma Bank	DSHB Cat# 5E1, RRID:AB_528466	1:5
Antibody	Anti-Nkx2.2 (Mouse Monoclonal)	Developmental Studies Hybridoma Bank	DSHB Cat# 74.5A5, RRID:AB_531794	1:5
Antibody	Anti-Hb9 (Mouse Monoclonal)	Developmental Studies Hybridoma Bank	DSHB Cat# 81.5C10, RRID:AB_2145209	1:5
Antibody	Anti-Nkx6.1 (Mouse Monoclonal)	Developmental Studies Hybridoma Bank	DSHB Cat# F55A10, RRID:AB_532378	1:50
Antibody	Anti-acetylated a-tubulin (Mouse Monoclonal)	Millipore Sigma	Sigma-Aldrich Cat# T6793, RRID:AB_477585	1:2500
Antibody	Anti-Olig2 (Rabbit Polyclonal)	Millipore Sigma	Millipore Cat# AB9610, RRID:AB_570666	1:300
Antibody	Anti-Arl13b (Mouse Monoclonal)	NeuroMab	UC Davis/NIH NeuroMab Facility Cat# 73-287, RRID:AB_11000053	1:1000
Antibody	Anti-Arl13b (Rabbit Polyclonal	Protein Tech	Proteintech Cat# 17711-1-AP, RRID:AB_2060867	1:1000
Antibody	Anti-Arl13b (Rabbit Polyclonal	PMID:17488627	503	1:1000
Antibody	Anti-Arl13b (Rabbit Polyclonal	PMID:17488627	504	1:1000
Antibody	Anti-Arl13b (Rabbit Polyclonal	PMID:17488627	505	1:1000

Antibody	Anti-Smo (Rabbit Polyclonal)	K. Anderson		1:1000
Antibody	Anti-IFT88 (Rabbit Polyclonal)	B. Yoder		1:1000
Antibody	Anti-Arl3 (Rabbit Polyclonal)	PMID:8034651		1:1000
Antibody	Anti-Inpp5e (Rabbit Polyclonal)	Protein Tech	Proteintech Cat# 17797-1-AP, RRID:AB_2167120	1:150
Antibody	Anti-Gli2 (Guinea Pig Polyclonal)	J. Eggenschwiler		1:200
Antibody	Anti-Gli3 (Goat Polyclonal)	R&D	R and D Systems Cat# AF3690, RRID:AB_2232499	1:200
Antibody	Anti-Ptch1 (Rabbit Polyclonal)	R. Rohatgi		1:150
Antibody	Anti-Sufu (Goat Polyclonal)	Santa Cruz	Santa Cruz Biotechnology Cat# sc-10933, RRID:AB_671172	1:100
Antibody	Alexa Fluor goat anti-mouse IgG2a 488	ThermoFisher	Thermo Fisher Scientific Cat# A-21131, RRID:AB_2535771	1:300
Antibody	Alexa Fluor goat anti-mouse IgG1 488	ThermoFisher	Thermo Fisher Scientific Cat# A-21121, RRID:AB_2535764	1:300
Antibody	Alexa Fluor goat anti-mouse Ig 488	ThermoFisher	Molecular Probes Cat# A-11029, RRID:AB_138404	1:300

Antibody	Alexa Fluor goat anti-mouse IgG 568	ThermoFisher	Thermo Fisher Scientific Cat# A-11031, RRID:AB_144696	1:300
Antibody	Alexa Fluor donkey anti-rabbit IgG 488	ThermoFisher	Thermo Fisher Scientific Cat# A-21206, RRID:AB_2535792	1:300
Antibody	Alexa Fluor donkey anti-rabbit IgG 555	ThermoFisher	Thermo Fisher Scientific Cat# A-31572, RRID:AB_162543	1:300
Antibody	Alexa Fluor goat anti-rabbit IgG 568	ThermoFisher	Thermo Fisher Scientific Cat# A-11011, RRID:AB_143157	1:300
Antibody	Alexa Fluor goat anti-mouse IgG2b 568	ThermoFisher	Thermo Fisher Scientific Cat# A-21147, RRID:AB_2535783	1:300
Antibody	Hoechst nuclear stain	Millipore Sigma	94403	1:3000
sequence-based reagent	CRISPR gRNA	Millpore Sigma, this paper		CCAGTCAATACAGACGAGTCTA
sequence-based reagent	CRISPR donor oligo	Millpore Sigma, this paper		CCTATATTCTTCTAGAAAACAGTAAGAAGAAAACCAAGAAACTACGAATGAAAAGGAGTCATCGGGCAGAACCAGTGAATACAGACGAGTCTACTCCAAAGAGTCCCACGC

				CTCCCCAAC
sequence-based reagent	F-231-Cac8I	This Paper		PCR Primer AAGAATGAAAAGGAGTCAGCG
sequence-based reagent	REV-1	This Paper		PCR Primer TGAACCGCTAATGGGAAACT
peptide, recombinant protein	Arl13b^{WT}-GST	This Paper		Purified from cells
peptide, recombinant protein	Arl13b^{V358A}-GST	This Paper		Purified from cells
peptide, recombinant protein	Arl3 (human)	PMID:11303027		Purified from cells
peptide, recombinant protein	Cas9	Millipore Sigma	C120010	50 μg
peptide, recombinant protein	Cac8I	New England Biolabs	R0579L	Restriction enzyme
chemical compound, drug	Ciliobrevin-D	Millipore Sigma	250401	30 μM
chemical compound, drug	[3H]GDP	PerkinElmer Life Sciences	NET966	3,000 cpm/pmol
chemical compound, drug	GTPgS35	PerkinElmer Life Sciences	NEG030H	
Software, algorithm	ImageJ software	ImageJ (http://imagej.nih.gov/ij/)	ImageJ, RRID:SCR_003070	

Software, algorithm	GraphPad Prism software	GraphPad Prism (Https://graphpad.com)	GraphPad Prism, RRID:SCR_002798	Version 8.0.0

Methods

Protein purification and ARL3 GEF assay

Plasmids directing the expression of mouse GST-ARL13B or GST-ARL13B^{V358A} proteins were transiently transfected into HEK cells and the recombinant proteins were later purified by affinity chromatography using glutathione-Sepharose, as described previously (Cavenagh et al. 1994; Ivanova et al. 2017). Human ARL3 (98.4% identical to mouse ARL3) was expressed in BL21 bacteria and purified as previously described (Van Valkenburgh et al. 2001). The ARL3 GEF assay was performed as previously described (Ivanova et al. 2017). Briefly, ARL3 (10μM) was pre-incubated with [^{3}H]GDP (1 μM; PerkinElmer Life Sciences, specific activity ~3,000 cpm/pmol) for 1 h at 30°C in 25 mM HEPES, pH 7.4, 100 mM NaCl, 10 mM $MgCl_2$. In contrast, pre-loading of ARL13B (10μM) was achieved by incubation in 100 μM GTPγS for 1 min at room temperature, due to its much more rapid exchange kinetics. The GEF assay was initiated upon addition of ARL3 (final = 1μM), ARL13B (final = 0 or 1μM), 10 μM GTPγS, and 100 μM GDP (to prevent re-binding of any released [^{3}H]GDP), in a final volume of 100 μL. The intrinsic rate of GDP dissociation from ARL3 was determined in parallel as that released in the absence of any added ARL13B. The reactions were stopped at different times (0–15 min) by dilution of 10μL of the reaction mixture into 2 ml of ice-cold buffer (20 mM Tris, pH 7.5, 100 mM NaCl, 10 mM $MgCl_2$, 1 mM dithiothreitol). The amount of ARL3-bound [^{3}H]GDP was determined by rapid filtration through BA85

nitrocellulose filters (0.45 μm, 25 mm, Whatman), with 3 x 2 mL washes, and quantified using liquid scintillation counting. Time points are routinely collected in at least duplicate and each experiment reported was repeated at least twice, yielding very similar results. Data were analyzed in GraphPad Prism 7 software.

Mouse allele generation and identification

All mice were cared for in accordance with NIH guidelines and Emory's Institutional Animal Care and Use Committee (IACUC). Lines used were *Arl13b*^{V358A} (*Arl13b*^{em1Tc}) [MGI: 6256969], *Arl13b*^{hnn} [MGI: 3578151] and FVB/NJ (Jackson Laboratory). To generate the V358A point mutation in the mouse, a CRISPR gRNA (CCAGTCAATACAGACGAGTCTA) targeting exon 8 of the *Arl13b* locus along with a donor oligo (5'-CCTATATTCTTCTAGAAAACAGTAAGAAGAAAACCAAGAAACTACGAATGAAAAGGAGTCATCGGGCAGAACCAGTGAATACAGACGAGTCTACTCCAAAGAGTCCCACGCCTCCCCAAC-3'; underlined bases are engineered) were designed to generate a T-to-C change creating the V358A point mutation and C-to-G change creating a TspRI restriction site that could be used for genotyping (Millipore Sigma). The gRNA (50 ng/μl), oligo donor (50 ng/μl) and CRISPR protein (100 ng/μL) were injected by the Emory Transgenic and Gene Targeting core into one-cell C57Bl/6J zygotes. Zygotes were cultured to 2-cell before being transferred to pseudopregnant females. Genomic tail DNA from resulting offspring was amplified using PCR primers (5'-GAAGCAGGCATGGTGGTAAT-3' & 5'-TGAACCGCTAATGGGAAATC-3') located upstream and downstream of the donor oligo breakpoints. The products were

sequenced (5'-GAAGCAGGCATGGTGGTAAT-3') and 2 animals were identified heterozygous for the desired change and with no additional editing. One line (#173) was bred to FVB/NJ for three generations prior to performing any phenotypic analysis. Males from at least two distinct meiotic recombination opportunities were used in each generation that to minimize potential confounds associated with off-target CRISPR/Cas9 editing.

Genotyping was performed on DNA extracted from ear punch or yolk sac via PCR using the following primers: Fwd: 5'- AAGAATGAAAAGGAGTCAGCG -3', Rev: 5'-TGAACCGCTAATGGGAAACT -3'; a SNP was engineered in the forward primer that, in combination with the V358A mutation, created a Cac8I restriction site. Thus, the PCR product was digested with Cac8I enzyme, run out on a 4% agarose gel and the relevant bands were detected: undigested wild type (~192bp) and digested mutant bands (~171bp).

Phenotypic analysis of embryos

Timed matings of heterozygous intercrosses were performed to generate embryos of the indicated stage, with somite-matched pairs examined at each stage when appropriate. Embryos were dissected in cold phosphate-buffered saline and processed for immunofluorescence staining as previously described (Horner et al. 2011).

Mouse embryonic fibroblasts

Mouse embryonic fibroblasts (MEFs) were isolated and immortalized as previously described (Mariani et al. 2016). The identity of all cell lines were confirmed by

494 genotyping PCR and tested mycoplasma negative. MEFs were maintained in DMEM
495 with 10% fetal bovine serum (FBS) and 1% penicillin/streptomycin at 37°C in 5% CO_2.
496 For experimental use, *Arl13b*$^{+/+}$, *Arl13b*$^{V358A/+}$, and *Arl13b*$^{V358A/V358A}$ and *Arl13b*$^{hnn/hnn}$
497 MEFs were grown on coverslips at a density of 0.5 x 10^6 cells/mL and treated for 24 h
498 with 0.5% FBS Shh conditioned media or 0.5% FBS media to induce ciliogenesis
499 (Larkins et al. 2011).
500
501 *Antibodies*
502 Primary antibodies used were: mouse anti-Shh (5E1), mouse anti-Nkx2.2 (74.5A5),
503 mouse anti-HB9 (81.5C10), mouse anti-Nkx6.1 (F55A10) (1:5 Developmental Studies
504 Hybridoma Bank); rabbit anti-Olig2 (1:300 Millipore AB9610); mouse anti-acetylated α-
505 tubulin (1:2500 Millipore Sigma; T6793), mouse anti-ARL13B (1:1000 NeuroMab
506 N295B/66), rabbit anti-ARL13B (1:1000, Protein Tech 17711-1-AP); rabbit anti-ARL13B
507 sera from 3 distinct rabbits (503, 504 and 505) (Caspary Lab (Caspary et al. 2007)),
508 rabbit anti-Smoothened (1:1000, kindly provided by K. Anderson); rabbit anti-IFT88
509 (1:1000, kindly provided by B. Yoder); rabbit anti-ARL3 (1:1000, (Cavenagh et al.
510 1994)); rabbit anti- INPP5E (1:150, Protein Tech 17797-1-AP); guinea pig anti-Gli2
511 (1:200, kindly provided by J. Eggenschwiler); rabbit anti-Ptch1 (1:150, kindly provided
512 by R. Rohatgi), goat anti-Sufu (1:100, SC10933, Santa Cruz); goat anti-Gli3 (1:200,
513 R&D AF3690); Alexa Fluor 488 and Alexa Fluor 568 (1:300, ThermoFisher); and
514 Hoechst nuclear stain (1:3000). In all depicted images the red channel is false colored
515 as magenta for the benefit of readers.
516

Image Quantification

Fluorescent intensities were measured in ImageJ software. Cilia were first identified by positive acetylated α-tubulin and an outline was hand drawn around the length of the cilium. The channel was switched to the protein of interest and a measurement of the average fluorescent intensity was acquired. The same outline was then used to acquire a background reading of the cell-body that most closely matched the background at the cilium. In all cases immunofluorescent averages of proteins of interest in cilia were normalized to cell-body intensities (Figure 3 – Figure supplement 1). For samples with antibodies targeting Gli2, Gli3, and Sufu the ciliary tip was isolated and measured. The cilia tip was identified by weak acetylated α-tubulin staining or the cilium base was identified by the presence of the acetylated α-tubulin positive fibrils in the cell body that cluster at the base of the cilium (Larkins et al. 2011). For samples with antibodies targeting Smo, Ptch1, ARL3, and INPP5E the entire cilium was measured. We plotted the ratio of fluorescence intensity of the protein of interest to the cell body background as violin plots. Within each plot the dashed lines represent the median and interquartile range. The number of cilia examined per genotype and per condition are listed below their respective plot. All data, except for Smo which varied both genotype and treatment, were analyzed by one-way ANOVA. In the event of a significant ANOVA, Tukey's multiple comparisons were employed to determine significance as all groups were compared. Smo fluorescent intensity data were analyzed by two-way ANOVA. As only specific groups were compared, the significance of those comparisons across and between groups were made using Sidak's post-hoc to not inflate the significance of those comparisons Data were analyzed in GraphPad Prism 7 software.

In a similar experiment, retrograde IFT was inhibited by the addition of 30 μM ciliobrevin-D (Millipore Sigma; 250401) or 0.1% DMSO control in low-serum media for 60 min after ciliation was induced by serum starvation for 24 h prior with 0.5% FBS media. Cilia were identified by staining with antibodies directed against acetylated α-tubulin, IFT88, and ARL13B. Fluorescent intensities were measured in ImageJ software. Again, cilia were first identified by positive acetylated α-tubulin and an outline was hand drawn. The channel was switched to the protein of interest and a measurement of the average fluorescent intensity was acquired. The same outline was then used to acquire a background reading of the cell-body. To measure IFT88, the cilia tip was identified by weak acetylated α-tubulin staining or the cilium base was identified by the presence of acetylated α-tubulin fibrils in the cell body that cluster at the base of the cilium (Larkins et al. 2011). To make comparisons among cell lines of distinct genotype with and without ciliobrevin-D treatment, data were analyzed by two-way ANOVA. To analyze the specific differences across groups, multiple comparisons were made using Sidak's post-hoc.

Western Blots

Western blotting was performed as previously described (Mariani et al. 2016), with antibody against ARL13B (1:1000 Neuromab N295B/66). Lysates were prepared with RIPA buffer and SigmaFast protease inhibitors (Nachtergaele et al. 2013). Values presented as volume intensity measured by chemiluminescence detected on ChemiDoc Touch Imaging System were normalized to total protein as measured on a stain-free gel (Thacker et al. 2016; Rivero-Gutierrez et al. 2014). Normalized values were analyzed by

one-way ANOVA and Tukey's multiple comparisons. Data were analyzed in GraphPad Prism 7 software.

Materials in this manuscript are available, those interested should contract the corresponding author.

Acknowledgements

This work was supported by funding from NIH grants R01NS090029 and R35GM122549 to T.C. and R35GM122568 to R.A.K. E.D.G. was supported by NIH training grant T32NS096050 and a diversity supplement to R01NS090029. Further support came from the Emory Integrated Mouse Transgenic and Gene Targeting Core, which is subsidized by the Emory University School of Medicine and with support by the Georgia Clinical & Translational Science Alliance of the National Institutes of Health under Award Number UL1TR002378 as well as the Emory University Integrated Cellular Imaging Microscopy Core of the Emory Neuroscience NINDS Core Facilities grant, P30NS055077. We are grateful to Alyssa Long and Sarah Suciu for sequencing potential CRISPR founders, and to members of the Caspary lab for discussion and manuscript comments.

Competing Interests

The authors have no competing interests to disclose.

References

Aza-Blanc, P., H. Y. Lin, A. Ruiz i Altaba, and T. B. Kornberg. 2000. 'Expression of the vertebrate Gli proteins in Drosophila reveals a distribution of activator and repressor activities', *Development*, 127: 4293-301.

Bangs, F. K., N. Schrode, A. K. Hadjantonakis, and K. V. Anderson. 2015. 'Lineage specificity of primary cilia in the mouse embryo', *Nat Cell Biol*, 17: 113-22.

Barral, D. C., S. Garg, C. Casalou, G. F. Watts, J. L. Sandoval, J. S. Ramalho, V. W. Hsu, and M. B. Brenner. 2012. 'Arl13b regulates endocytic recycling traffic', *Proc Natl Acad Sci U S A*, 109: 21354-9.

Bay, S. N., A. B. Long, and T. Caspary. 2018. 'Disruption of the ciliary GTPase Arl13b suppresses Sonic hedgehog overactivation and inhibits medulloblastoma formation', *Proc Natl Acad Sci U S A*, 115: 1570-75.

Briscoe, J., Y. Chen, T. M. Jessell, and G. Struhl. 2001. 'A hedgehog-insensitive form of patched provides evidence for direct long-range morphogen activity of sonic hedgehog in the neural tube', *Mol Cell*, 7: 1279-91.

Briscoe, J., and P. P. Therond. 2013. 'The mechanisms of Hedgehog signalling and its roles in development and disease', *Nat Rev Mol Cell Biol*, 14: 416-29.

Casalou, C., C. Seixas, A. Portelinha, P. Pintado, M. Barros, J. S. Ramalho, S. S. Lopes, and D. C. Barral. 2014. 'Arl13b and the non-muscle myosin heavy chain IIA are required for circular dorsal ruffle formation and cell migration', *J Cell Sci*, 127: 2709-22.

Caspary, T., C. E. Larkins, and K. V. Anderson. 2007. 'The graded response to Sonic Hedgehog depends on cilia architecture', *Dev Cell*, 12: 767-78.

Cavenagh, M. M., M. Breiner, A. Schurmann, A. G. Rosenwald, T. Terui, C. Zhang, P. A. Randazzo, M. Adams, H. G. Joost, and R. A. Kahn. 1994. 'ADP-ribosylation factor (ARF)-like 3, a new member of the ARF family of GTP-binding proteins cloned from human and rat tissues', *J Biol Chem*, 269: 18937-42.

Cevik, S., Y. Hori, O. I. Kaplan, K. Kida, T. Toivenon, C. Foley-Fisher, D. Cottell, T. Katada, K. Kontani, and O. E. Blacque. 2010. 'Joubert syndrome Arl13b functions at ciliary membranes and stabilizes protein transport in Caenorhabditis elegans', *J Cell Biol*, 188: 953-69.

Cevik, S., A. A. Sanders, E. Van Wijk, K. Boldt, L. Clarke, J. van Reeuwijk, Y. Hori, N. Horn, L. Hetterschijt, A. Wdowicz, A. Mullins, K. Kida, O. I. Kaplan, S. E. van Beersum, K. Man Wu, S. J. Letteboer, D. A. Mans, T. Katada, K. Kontani, M. Ueffing, R. Roepman, H. Kremer, and O. E. Blacque. 2013. 'Active transport and diffusion barriers restrict Joubert Syndrome-associated ARL13B/ARL-13 to an Inv-like ciliary membrane subdomain', *PLoS Genet*, 9: e1003977.

Chavez, M., S. Ena, J. Van Sande, A. de Kerchove d'Exaerde, S. Schurmans, and S. N. Schiffmann. 2015. 'Modulation of Ciliary Phosphoinositide Content Regulates Trafficking and Sonic Hedgehog Signaling Output', *Dev Cell*, 34: 338-50.

Chiang, C., Y. Litingtung, E. Lee, K. E. Young, J. L. Corden, H. Westphal, and P. A. Beachy. 1996. 'Cyclopia and defective axial patterning in mice lacking Sonic hedgehog gene function', *Nature*, 383: 407-13.

Consortium, C. elegans Sequencing. 1998. 'Genome sequence of the nematode C. elegans: a platform for investigating biology', *Science*, 282: 2012-8.

Corbit, K. C., P. Aanstad, V. Singla, A. R. Norman, D. Y. Stainier, and J. F. Reiter. 2005. 'Vertebrate Smoothened functions at the primary cilium', *Nature*, 437: 1018-21.

626 Cortellino, S., C. Wang, B. Wang, M. R. Bassi, E. Caretti, D. Champeval, A. Calmont, M.
627 Jarnik, J. Burch, K. S. Zaret, L. Larue, and A. Bellacosa. 2009. 'Defective ciliogenesis,
628 embryonic lethality and severe impairment of the Sonic Hedgehog pathway caused by
629 inactivation of the mouse complex A intraflagellar transport gene Ift122/Wdr10, partially
630 overlapping with the DNA repair gene Med1/Mbd4', *Dev Biol*, 325: 225-37.
631 D'Souza-Schorey, C., and P. Chavrier. 2006. 'ARF proteins: roles in membrane traffic and
632 beyond', *Nat Rev Mol Cell Biol*, 7: 347-58.
633 Dessaud, E., L. L. Yang, K. Hill, B. Cox, F. Ulloa, A. Ribeiro, A. Mynett, B. G. Novitch, and J.
634 Briscoe. 2007. 'Interpretation of the sonic hedgehog morphogen gradient by a temporal
635 adaptation mechanism', *Nature*, 450: 717-20.
636 Dyson, J. M., S. E. Conduit, S. J. Feeney, S. Hakim, T. DiTommaso, A. J. Fulcher, A. Sriratana,
637 G. Ramm, K. A. Horan, R. Gurung, C. Wicking, I. Smyth, and C. A. Mitchell. 2017.
638 'INPP5E regulates phosphoinositide-dependent cilia transition zone function', *J Cell Biol*,
639 216: 247-63.
640 East, M. P., J. B. Bowzard, J. B. Dacks, and R. A. Kahn. 2012. 'ELMO domains, evolutionary
641 and functional characterization of a novel GTPase-activating protein (GAP) domain for
642 Arf protein family GTPases', *J Biol Chem*, 287: 39538-53.
643 Firestone, A. J., J. S. Weinger, M. Maldonado, K. Barlan, L. D. Langston, M. O'Donnell, V. I.
644 Gelfand, T. M. Kapoor, and J. K. Chen. 2012. 'Small-molecule inhibitors of the AAA+
645 ATPase motor cytoplasmic dynein', *Nature*, 484: 125-9.
646 Garcia-Gonzalo, F. R., S. C. Phua, E. C. Roberson, G. Garcia, 3rd, M. Abedin, S. Schurmans, T.
647 Inoue, and J. F. Reiter. 2015. 'Phosphoinositides Regulate Ciliary Protein Trafficking to
648 Modulate Hedgehog Signaling', *Dev Cell*, 34: 400-09.
649 Goetz, S. C., P. J. Ocbina, and K. V. Anderson. 2009. 'The primary cilium as a Hedgehog signal
650 transduction machine', *Methods Cell Biol*, 94: 199-222.
651 Gotthardt, K., M. Lokaj, C. Koerner, N. Falk, A. Giessl, and A. Wittinghofer. 2015. 'A G-protein
652 activation cascade from Arl13B to Arl3 and implications for ciliary targeting of lipidated
653 proteins', *Elife*, 4.
654 Hanke-Gogokhia, C., Z. Wu, C. D. Gerstner, J. M. Frederick, H. Zhang, and W. Baehr. 2016.
655 'Arf-like Protein 3 (ARL3) Regulates Protein Trafficking and Ciliogenesis in Mouse
656 Photoreceptors', *J Biol Chem*, 291: 7142-55.
657 Haycraft, C. J., B. Banizs, Y. Aydin-Son, Q. Zhang, E. J. Michaud, and B. K. Yoder. 2005. 'Gli2
658 and Gli3 localize to cilia and require the intraflagellar transport protein polaris for
659 processing and function', *PLoS Genet*, 1: e53.
660 Higginbotham, H., T. Y. Eom, L. E. Mariani, A. Bachleda, J. Hirt, V. Gukassyan, C. L. Cusack,
661 C. Lai, T. Caspary, and E. S. Anton. 2012. 'Arl13b in primary cilia regulates the
662 migration and placement of interneurons in the developing cerebral cortex', *Dev Cell*, 23:
663 925-38.
664 Hori, Y., T. Kobayashi, Y. Kikko, K. Kontani, and T. Katada. 2008. 'Domain architecture of the
665 atypical Arf-family GTPase Arl13b involved in cilia formation', *Biochem Biophys Res*
666 *Commun*, 373: 119-24.
667 Horner, V. L., and T. Caspary. 2011. 'Disrupted dorsal neural tube BMP signaling in the cilia
668 mutant Arl13b hnn stems from abnormal Shh signaling', *Dev Biol*, 355: 43-54.
669 Houde, C., R. J. Dickinson, V. M. Houtzager, R. Cullum, R. Montpetit, M. Metzler, E. M.
670 Simpson, S. Roy, M. R. Hayden, P. A. Hoodless, and D. W. Nicholson. 2006. 'Hippi is
671 essential for node cilia assembly and Sonic hedgehog signaling', *Dev Biol*, 300: 523-33.

672 Huangfu, D., and K. V. Anderson. 2005. 'Cilia and Hedgehog responsiveness in the mouse', *Proc*
673 *Natl Acad Sci U S A*, 102: 11325-30.
674 Huangfu, D., A. Liu, A. S. Rakeman, N. S. Murcia, L. Niswander, and K. V. Anderson. 2003.
675 'Hedgehog signalling in the mouse requires intraflagellar transport proteins', *Nature*, 426:
676 83-7.
677 Huangfu, Danwei, and Kathryn V Anderson. 2006. 'Signaling from Smo to Ci/Gli: conservation
678 and divergence of Hedgehog pathways from Drosophila to vertebrates', *Development*,
679 133: 3-14.
680 Humbert, M. C., K. Weihbrecht, C. C. Searby, Y. Li, R. M. Pope, V. C. Sheffield, and S. Seo.
681 2012. 'ARL13B, PDE6D, and CEP164 form a functional network for INPP5E ciliary
682 targeting', *Proc Natl Acad Sci U S A*, 109: 19691-6.
683 Humke, E. W., K. V. Dorn, L. Milenkovic, M. P. Scott, and R. Rohatgi. 2010. 'The output of
684 Hedgehog signaling is controlled by the dynamic association between Suppressor of
685 Fused and the Gli proteins', *Genes Dev*, 24: 670-82.
686 Ingham, P. W., Y. Nakano, and C. Seger. 2011. 'Mechanisms and functions of Hedgehog
687 signalling across the metazoa', *Nat Rev Genet*, 12: 393-406.
688 Ivanova, A. A., T. Caspary, N. T. Seyfried, D. M. Duong, A. B. West, Z. Liu, and R. A. Kahn.
689 2017. 'Biochemical characterization of purified mammalian ARL13B protein indicates
690 that it is an atypical GTPase and ARL3 guanine nucleotide exchange factor (GEF)', *J Biol*
691 *Chem*, 292: 11091-108.
692 Kahn, R. A., E. Bruford, H. Inoue, J. M. Logsdon, Jr., Z. Nie, R. T. Premont, P. A. Randazzo, M.
693 Satake, A. B. Theibert, M. L. Zapp, and D. Cassel. 2008. 'Consensus nomenclature for
694 the human ArfGAP domain-containing proteins', *J Cell Biol*, 182: 1039-44.
695 Kim, J., M. Kato, and P. A. Beachy. 2009. 'Gli2 trafficking links Hedgehog-dependent activation
696 of Smoothened in the primary cilium to transcriptional activation in the nucleus', *Proc*
697 *Natl Acad Sci U S A*, 106: 21666-71.
698 Kong, J. H., C. Siebold, and R. Rohatgi. 2019. 'Biochemical mechanisms of vertebrate hedgehog
699 signaling', *Development*, 146.
700 Kuwabara, P. E., M. H. Lee, T. Schedl, and G. S. Jefferis. 2000. 'A C. elegans patched gene, ptc-
701 1, functions in germ-line cytokinesis', *Genes Dev*, 14: 1933-44.
702 Larkins, C. E., G. D. Aviles, M. P. East, R. A. Kahn, and T. Caspary. 2011. 'Arl13b regulates
703 ciliogenesis and the dynamic localization of Shh signaling proteins', *Mol Biol Cell*, 22:
704 4694-703.
705 Li, Y., W. G. Kelly, J. M. Logsdon, Jr., A. M. Schurko, B. D. Harfe, K. L. Hill-Harfe, and R. A.
706 Kahn. 2004. 'Functional genomic analysis of the ADP-ribosylation factor family of
707 GTPases: phylogeny among diverse eukaryotes and function in C. elegans', *FASEB J*, 18:
708 1834-50.
709 Li, Y., Q. Wei, Y. Zhang, K. Ling, and J. Hu. 2010. 'The small GTPases ARL-13 and ARL-3
710 coordinate intraflagellar transport and ciliogenesis', *J Cell Biol*, 189: 1039-51.
711 Liem, K. F., Jr., A. Ashe, M. He, P. Satir, J. Moran, D. Beier, C. Wicking, and K. V. Anderson.
712 2012. 'The IFT-A complex regulates Shh signaling through cilia structure and membrane
713 protein trafficking', *J Cell Biol*, 197: 789-800.
714 Liem, K. F., Jr., M. He, P. J. Ocbina, and K. V. Anderson. 2009. 'Mouse Kif7/Costal2 is a cilia-
715 associated protein that regulates Sonic hedgehog signaling', *Proc Natl Acad Sci U S A*,
716 106: 13377-82.

717 Lim, Y. S., C. E. Chua, and B. L. Tang. 2011. 'Rabs and other small GTPases in ciliary
718 transport', *Biol Cell*, 103: 209-21.
719 Liu, A., B. Wang, and L. A. Niswander. 2005. 'Mouse intraflagellar transport proteins regulate
720 both the activator and repressor functions of Gli transcription factors', *Development*, 132:
721 3103-11.
722 Logsdon, J. M., Jr., and R. A. Kahn (ed.)^(eds.). 2004. *Arf Family GTPases. In: Kahn RA, editor*.
723 Lu, H., M. T. Toh, V. Narasimhan, S. K. Thamilselvam, S. P. Choksi, and S. Roy. 2015. 'A
724 function for the Joubert syndrome protein Arl13b in ciliary membrane extension and
725 ciliary length regulation', *Dev Biol*, 397: 225-36.
726 Mariani, L. E., M. F. Bijlsma, A. I. Ivanova, S. K. Suciu, R. A. Kahn, and T. Caspary. 2016.
727 'Arl13b regulates Shh signaling from both inside and outside the cilium', *Mol Biol Cell*.
728 Miertzschke, M., C. Koerner, M. Spoerner, and A. Wittinghofer. 2014. 'Structural insights into
729 the small G-protein Arl13B and implications for Joubert syndrome', *Biochem J*, 457: 301-
730 11.
731 Milenkovic, L., M. P. Scott, and R. Rohatgi. 2009. 'Lateral transport of Smoothened from the
732 plasma membrane to the membrane of the cilium', *J Cell Biol*, 187: 365-74.
733 Murdoch, J. N., and A. J. Copp. 2010. 'The relationship between sonic Hedgehog signaling, cilia,
734 and neural tube defects', *Birth Defects Res A Clin Mol Teratol*, 88: 633-52.
735 Murray, S. A., J. L. Morgan, C. Kane, Y. Sharma, C. S. Heffner, J. Lake, and L. R. Donahue.
736 2010. 'Mouse gestation length is genetically determined', *PLoS One*, 5: e12418.
737 Nachtergaele, S., D. M. Whalen, L. K. Mydock, Z. Zhao, T. Malinauskas, K. Krishnan, P. W.
738 Ingham, D. F. Covey, C. Siebold, and R. Rohatgi. 2013. 'Structure and function of the
739 Smoothened extracellular domain in vertebrate Hedgehog signaling', *Elife*, 2: e01340.
740 Nozaki, S., Y. Katoh, M. Terada, S. Michisaka, T. Funabashi, S. Takahashi, K. Kontani, and K.
741 Nakayama. 2017. 'Regulation of ciliary retrograde protein trafficking by the Joubert
742 syndrome proteins ARL13B and INPP5E', *J Cell Sci*, 130: 563-76.
743 Nusslein-Volhard, C., and E. Wieschaus. 1980. 'Mutations affecting segment number and
744 polarity in Drosophila', *Nature*, 287: 795-801.
745 Placzek, M., and J. Briscoe. 2018. 'Sonic hedgehog in vertebrate neural tube development', *Int J*
746 *Dev Biol*, 62: 225-34.
747 Raleigh, D. R., and J. F. Reiter. 2019. 'Misactivation of Hedgehog signaling causes inherited and
748 sporadic cancers', *J Clin Invest*, 129: 465-75.
749 Revenkova, E., Q. Liu, G. L. Gusella, and C. Iomini. 2018. 'The Joubert syndrome protein
750 ARL13B binds tubulin to maintain uniform distribution of proteins along the ciliary
751 membrane', *J Cell Sci*, 131.
752 Rink, J. C., K. A. Gurley, S. A. Elliott, and A. Sanchez Alvarado. 2009. 'Planarian Hh signaling
753 regulates regeneration polarity and links Hh pathway evolution to cilia', *Science*, 326:
754 1406-10.
755 Rivero-Gutierrez, B., A. Anzola, O. Martinez-Augustin, and F. S. de Medina. 2014. 'Stain-free
756 detection as loading control alternative to Ponceau and housekeeping protein
757 immunodetection in Western blotting', *Anal Biochem*, 467: 1-3.
758 Roelink, H., A. Augsburger, J. Heemskerk, V. Korzh, S. Norlin, A. Ruiz i Altaba, Y. Tanabe, M.
759 Placzek, T. Edlund, T. M. Jessell, and et al. 1994. 'Floor plate and motor neuron
760 induction by vhh-1, a vertebrate homolog of hedgehog expressed by the notochord', *Cell*,
761 76: 761-75.

762 Rohatgi, R., L. Milenkovic, and M. P. Scott. 2007. 'Patched1 regulates hedgehog signaling at the
763 primary cilium', *Science*, 317: 372-6.
764 Roy, S. 2012. 'Cilia and Hedgehog: when and how was their marriage solemnized?',
765 *Differentiation*, 83: S43-8.
766 Ruiz i Altaba, A. 1998. 'Combinatorial Gli gene function in floor plate and neuronal inductions
767 by Sonic hedgehog', *Development*, 125: 2203-12.
768 Schlacht, A., K. Mowbrey, M. Elias, R. A. Kahn, and J. B. Dacks. 2013. 'Ancient complexity,
769 opisthokont plasticity, and discovery of the 11th subfamily of Arf GAP proteins', *Traffic*,
770 14: 636-49.
771 Seixas, C., S. Y. Choi, N. Polgar, N. L. Umberger, M. P. East, X. Zuo, H. Moreiras, R.
772 Ghossoub, A. Benmerah, R. A. Kahn, B. Fogelgren, T. Caspary, J. H. Lipschutz, and D.
773 C. Barral. 2016. 'Arl13b and the exocyst interact synergistically in ciliogenesis', *Mol Biol*
774 *Cell*, 27: 308-20.
775 Sigg, Monika Abedin, Tabea Menchen, Chanjae Lee, Jeffery Johnson, Melissa K Jungnickel,
776 Semil P Choksi, Galo Garcia 3rd, Henriette Busengdal, Gerard W Dougherty, and Petra
777 Pennekamp. 2017. 'Evolutionary proteomics uncovers ancient associations of cilia with
778 signaling pathways', *Developmental cell*, 43: 744-62. e11.
779 Stolc, V., M. P. Samanta, W. Tongprasit, and W. F. Marshall. 2005. 'Genome-wide
780 transcriptional analysis of flagellar regeneration in Chlamydomonas reinhardtii identifies
781 orthologs of ciliary disease genes', *Proc Natl Acad Sci U S A*, 102: 3703-7.
782 Sztul, E., P. W. Chen, J. E. Casanova, J. Cherfils, J. B. Dacks, D. G. Lambright, F. S. Lee, P. A.
783 Randazzo, L. C. Santy, A. Schurmann, I. Wilhelmi, M. E. Yohe, and R. A. Kahn. 2019.
784 'ARF GTPases and their GEFs and GAPs: concepts and challenges', *Mol Biol Cell*, 30:
785 1249-71.
786 Taylor, S. P., T. J. Dantas, I. Duran, S. Wu, R. S. Lachman, Consortium University of
787 Washington Center for Mendelian Genomics, S. F. Nelson, D. H. Cohn, R. B. Vallee, and
788 D. Krakow. 2015. 'Mutations in DYNC2LI1 disrupt cilia function and cause short rib
789 polydactyly syndrome', *Nat Commun*, 6: 7092.
790 Thacker, J. S., D. H. Yeung, W. R. Staines, and J. G. Mielke. 2016. 'Total protein or high-
791 abundance protein: Which offers the best loading control for Western blotting?', *Anal*
792 *Biochem*, 496: 76-8.
793 Tran, P. V., C. J. Haycraft, T. Y. Besschetnova, A. Turbe-Doan, R. W. Stottmann, B. J. Herron,
794 A. L. Chesebro, H. Qiu, P. J. Scherz, J. V. Shah, B. K. Yoder, and D. R. Beier. 2008.
795 'THM1 negatively modulates mouse sonic hedgehog signal transduction and affects
796 retrograde intraflagellar transport in cilia', *Nat Genet*, 40: 403-10.
797 Tuz, K., R. Bachmann-Gagescu, D. R. O'Day, K. Hua, C. R. Isabella, I. G. Phelps, A. E.
798 Stolarski, B. J. O'Roak, J. C. Dempsey, C. Lourenco, A. Alswaid, C. G. Bonnemann, L.
799 Medne, S. Nampoothiri, Z. Stark, R. J. Leventer, M. Topcu, A. Cansu, S. Jagadeesh, S.
800 Done, G. E. Ishak, I. A. Glass, J. Shendure, S. C. Neuhauss, C. R. Haldeman-Englert, D.
801 Doherty, and R. J. Ferland. 2014. 'Mutations in CSPP1 cause primary cilia abnormalities
802 and Joubert syndrome with or without Jeune asphyxiating thoracic dystrophy', *Am J Hum*
803 *Genet*, 94: 62-72.
804 Van Valkenburgh, H., J. F. Shern, J. D. Sharer, X. Zhu, and R. A. Kahn. 2001. 'ADP-ribosylation
805 factors (ARFs) and ARF-like 1 (ARL1) have both specific and shared effectors:
806 characterizing ARL1-binding proteins', *J Biol Chem*, 276: 22826-37.

807 Wang, Y., Z. Zhou, C. T. Walsh, and A. P. McMahon. 2009. 'Selective translocation of
808 intracellular Smoothened to the primary cilium in response to Hedgehog pathway
809 modulation', *Proc Natl Acad Sci U S A*, 106: 2623-8.
810 Warner, J. F., A. M. McCarthy, R. L. Morris, and D. R. McClay. 2014. 'Hedgehog signaling
811 requires motile cilia in the sea urchin', *Mol Biol Evol*, 31: 18-22.
812 Wen, X., C. K. Lai, M. Evangelista, J. A. Hongo, F. J. de Sauvage, and S. J. Scales. 2010.
813 'Kinetics of hedgehog-dependent full-length Gli3 accumulation in primary cilia and
814 subsequent degradation', *Mol Cell Biol*, 30: 1910-22.
815 Zhang, Q., Y. Li, Y. Zhang, V. E. Torres, P. C. Harris, K. Ling, and J. Hu. 2016. 'GTP-binding
816 of ARL-3 is activated by ARL-13 as a GEF and stabilized by UNC-119', *Sci Rep*, 6:
817 24534.
818 Zugasti, O., J. Rajan, and P. E. Kuwabara. 2005. 'The function and expansion of the Patched- and
819 Hedgehog-related homologs in C. elegans', *Genome Res*, 15: 1402-10.
820

Figure Legends

Figure 1.

ARL3 GEF activity is retained in the ARL13B^{V358A} mutant. Time course of the release of pre-bound [^{3}H]GDP from purified, recombinant ARL3 in the absence (ARL3) or presence of mouse wild type ARL13B or ARL13B^{V358A} (mARL13B) are shown. See Methods for details. Error bars ± standard deviation.

Figure 2.

Generation of the *Arl13b$^{V358A/V358A}$* mouse.

(A) Schematic of *Arl13b* gene and donor oligo (orange bar) at exon 8 used to generate the V358A causing point mutation. Arrows indicate primers used for allele validation. (B) *Arl13b* DNA and relevant amino acid sequence with the RVEP sequence in the orange box and the T-to-C mutation highlighted in pink. (C) Confocal images of cilia marker IFT88 (green) and ARL13B (magenta; NeuroMab) staining in neural tube of E10.5 somite-matched embryos. ARL13B-positive cilia are visible in *Arl13b$^{+/+}$* and *Arl13b$^{V358A/+}$*, but not in *Arl1b$^{V358A/V358A}$* embryos. (See Figure 2 – Figure supplement 1 for images of neural tube cilia under saturating conditions.) At least 5 embryos per genotype across five litters were examined. Scale bars are 50 μm. (D) ARL13B Western blot of E10.5 whole embryo lysates, wild type (+/+), *Arl13b$^{V358A/+}$* (*A*/+) and *Arl13b$^{V358A/V358A}$* (*A/A*) and (E) quantification presented as average intensity normalized to total protein ± standard deviation. Representative blot of whole embryo lysates (n = 3 embryos per genotype with technical duplicate of each). * $p < 0.05$, one-way ANOVA and Tukey's multiple comparison.

Figure 3.

ARL13B^{V358A} is undetectable in cilia and cannot be enriched by inhibition of retrograde transport.

(A) Antibodies against ciliary markers acetylated α-tubulin or IFT88 (magenta) and ARL13B (cyan) in *Arl13b$^{V358A/V358A}$* MEFs. Representative images show staining for five indicated ARL13B antibodies: (PT) polyclonal rabbit antibody against full-length human ARL13B from ProteinTech, (503, 504, 505) polyclonal rabbit sera from three distinct rabbits raised against C-terminus of mouse ARL13B (amino acids 208-427) (Caspary et al. 2007), and (NM) monoclonal mouse antibody against C terminus of mouse ARL13B from NeuroMab. *Arl13b$^{+/+}$* and *Arl13b$^{V358A/+}$* show ciliary ARL13B staining. Table lists ARL13B-positive cilia and the total number of cilia identified by acetylated α-tubulin or IFT88 antibody in parentheses. Cilia appear shorter in *Arl13b$^{V358A/V358A}$* cells (see Fig. 6). (B) IFT88 and (C) Gli3 (green) is enriched in the tips of cilia in *Arl13b$^{+/+}$* (+/+), *Arl13b$^{V358A/+}$* (*A*/+) and *Arl13b$^{V358A/V358A}$* (*A/A*) cells following ciliobrevin-D treatment. Violin plots depict relative fluorescence of IFT88 and Gli3 at cilia tip to cell body with number of cilia measured (n) listed beneath each plot. (D & E) Table lists ARL13B (cyan) positive cilia (rabbit anti-ARL13B; ProteinTech or mouse anti-ARL13B; NeuroMab) and the total number of cilia (acetylated α-tubulin: magenta) examined in control (DMSO) and ciliobrevin-D treated (30μM CB) cell lines. Representative images show staining for cilia and ARL13B. Staining of IFT88 and Gli3 analyzed by two-way ANOVA and Sidak's multiple comparisons. (*** $p < 0.001$, **** $p < 0.0001$).

Figure 4.

ARL13B^{V358A} mediates normal Shh signaling and neural tube patterning.

(A-I) Whole embryo and neural tube sections of somite-matched littermates at E9.5, E10.5, and E12.5 stained with indicated markers of cell fate. Whole embryo scale bars: 2 mm. (A'-I' & A"-F") Shh-dependent neural tube patterning at three separate time points. Cell fate markers are listed above each image. All neural tube scale bars are 50 μm. Neural tube patterning was examined in five embryos for each embryonic stage. E, embryonic day.

Figure 5.

ARL13B^{V358A} mediates normal ciliary enrichment of Shh components, but not ARL3 or INPP5E.

(A) Smo (green) enrichment in ventral neural tube cilia (acetylated α-tubulin: magenta) is normal in E10.5 embryos. Images are confocal projections. Scale bar is 25 μm. (B-H, Top) Quantification of average fluorescence intensity in the tip of the cilium (Gli2, Gli3, and Sufu) or the entire cilium (Ptch1, Smo, ARL3, and INPP5E) relative to background level. Violin plots depict relative fluorescent intensity per cilium with number of cilia examined below each plot. (B-H, Bottom) Representative images for each condition and cell type with the cilia marker acetylated α-tubulin (magenta) and indicated protein (green). Wild type (+/+), heterozygous (*A/+*), homozygous (*A/A)* and *hennin* (*hnn)*. Data analyzed by one-way ANOVA and Tukey's multiple comparisons, except Smo data analyzed by two-way ANOVA and 16 comparisons, corrected $p < 0.003$ deemed significant. (** $p < 0.01$, *** $p < 0.001$, **** $p < 0.0001$).

Figure 6.

ARL13B^{V358A} results in decreased ciliation rates and short cilia.

(A) Quantification of ciliation rates in all cell types; wild type (+/+), heterozygous (*A/+*), homozygous (*A/A)* and *hennin* (*hnn)*. Fewer *Arl13b$^{V358A/V358A}$* and *Arl13b$^{hnn/hnn}$* MEFs form cilia compared to *Arl13b$^{+/+}$* or *Arl13b$^{V358A/+}$* cells. (B) Quantification of axoneme length as labeled by acetylated α-tubulin (magenta) in indicated MEFs. Data are presented as mean (μm) ± standard deviation with the number of cilia measured per genotype depicted at the base of each bar. Data analyzed by one-way ANOVA and Tukey's multiple comparisons. (* $p < 0.05$, ** $p < 0.01$, *** $p < 0.001$, **** $p < 0.0001$)

Figure 7.

Model comparing complete loss of ARL13B function to ciliary loss of ARL13B function

Wildtype (left), *Arl13b^{hnnhnn}* (middle), and *Arl13b$^{V358A/V358A}$* (right) cilia represented as two halves. On the left half is the organization of Shh components in the presence of Shh ligand and on the right half is the organization of ARL13B interactors ARL3 and INPP5E. (A) ARL13B associates with the ciliary membrane. In the presence of Shh, Ptch1 is removed from cilia and Smo is visibly enriched in cilia. Smo is activated which promotes the processing of full-length Gli transcription factors into their activator forms (GliA), that are shuttled out of the cilium to promote Shh-dependent gene transcription. In addition, cilia proteins ARL3 and INPP5E are localized to the primary cilium. (B) In *Arl13b$^{hnn/hnn}$* cells which are null for ARL13B, cilia are shorter than normal. Ciliary Ptch1 and Smo are visible, although Smo appears punctate instead of diffuse. In addition, loss

of ARL13B decreases transcription of Shh-dependent genes due to lowered GliA. *Arl13b*$^{hnn/hnn}$ cilia also display a failure of INPP5E and ARL3 to localize to the cilium. Because ARL13B is the GEF for ARL3, we speculate in this schematic that ARL3 remains GDP bound in *Arl13b*$^{hnn/hnn}$ cells. (C) In *Arl13b*$^{V358A/V358A}$ cells, ARL13B^{V358A} is not detectable in cilia and appears diffuse within the cell body. *Arl13b*$^{V358A/V358A}$ cilia, like *Arl13b*$^{hnn/hnn}$ cilia, are shorter than wildtype. We observe normal Shh-dependent ciliary Smo enrichment and normal Shh transcriptional output. However, ARL3 and INPP5E are absent from cilia, indicating that ciliary ARL13B is required for ciliary residence of these proteins.

MICE	Sex	wildtype	*V358A/+*	*V358A/V358A*	
Het x Het	M (46.5%)	3	11	6	
Avg. Litter	F (53.5%)	6	8	9	
7.3	% of Total	20.9	44.2	34.9	$\chi^2 = 0.60$
Het x Hom	M (60%)	-	10	11	
Avg. Litter	F (40%)	-	6	8	
7.5	% of Total	-	45.7	54.3	$\chi^2 = 0.69$
Hom x Hom	M (47.4%)	-	-	9	
Avg. Litter	F (52.6%)	-	-	10	
9.5					

Table 1.

Genotype of mice born to heterozygous and/or homozygous carrier parents. Data analyzed by chi-squared test.

Figure 2 – Supplement 1

Overexposure of *Arl13b*$^{V358A/V358A}$ cilia in E10.5 neural tube reveals no clear ARL13B^{V358A} presence in cilia.

Overexposure of cilia in E10.5 *Arl13b*$^{+/+}$, *Arl13b*$^{V358A/V358A}$, and *Arl13b*$^{hnn/hnn}$ embryonic neural tube, stained for IFT88 and ARL13B (NeuroMab). The ARL13B channel was overexposed for four seconds instead of one second.

Figure 2 – Supplement 2

Overexposure of *Arl13b*$^{V358A/V358A}$ cilia in MEFs reveals no clear ARL13B^{V358A} presence in cilia.

(A) We identified acetylated α-tubulin positive cilia and used the marker to outline the area of the cilium. We quantified ARL13B immunofluorescence detected by Caspary lab polyclonal anti-ARL13B antibody (Caspary et al. 2007) and used the same trace to measure background levels in a different area of the cell body. (B) *Arl13b*$^{V358A/V358A}$ (*A/A*) and *Arl13b*$^{hnn/hnn}$ (*hnn*) MEFs treated with control or ciliobrevin-D 0.5% FBS Media. Samples were overexposed five times longer than normal, saturating the detector in the ARL13B channel. We measured no difference in ciliary ARL13B immunofluorescence between control and ciliobrevin-D treated *Arl13b*$^{V358A/V358A}$ and *Arl13b*$^{hnn/hnn}$ MEFs. Data presented as violin plots and analyzed by one-way ANOVA. Respective number of cilia listed below each plot. Cilia that had ARL13B immunofluorescent readings above background (*) are shown in panel D. (C) Representative images of over exposed *Arl13b*$^{V358A/V358A}$ and *Arl13b*$^{hnn/hnn}$ MEFs in

930 control and ciliobrevin-D treatment conditions. (D) Representative images of cilia with
931 ARL13B levels above background, marked by * in panel B.
932

Figure 3 – Supplement 1

933 **Endogenous ARL13B is undetectable in the cell body of cilia mutant *IFT172^{wim}***
934 **cells.**

935 Immunofluorescent detection of ARL13B (cyan; NeuroMab) and cilia marker acetylated
936 α-tubulin (magenta) in wildtype, *Arl13b^{hnn}*, *IFT172^{wim}*, and *IFT172^{wim} Arl13b^{hnn}* cell lines.
937 (A) In wildtype cells, ARL13B is detectable in the cilium under non-saturating conditions,
938 these parameters are kept constant across all samples. (B) In *IFT172^{wim}* non-ciliated
939 cells, ARL13B protein is confined to the cell body, but is nearly undetectable by
940 standard immunofluorescence. (C-D) In *Arl13b^{hnn}* and *IFT172^{wim} Arl13b^{hnn}* cells, null for
941 *Arl13b*, any signal is due primary antibody background. At an exposure rate 4x above
942 normal the ARL13B signal saturates the detector in wildtype cells. In *IFT172^{wim}* cells,
943 overexposure reveals no ARL13B positive stain that is above the background detected
944 in *Arl13b^{hnn}* and *IFT172^{wim} Arl13b^{hnn}* cells. Images taken at 40x. Scale bar is 5 μm.
945 Experiments repeated in duplicate and examined 4-6 fields of view per condition.

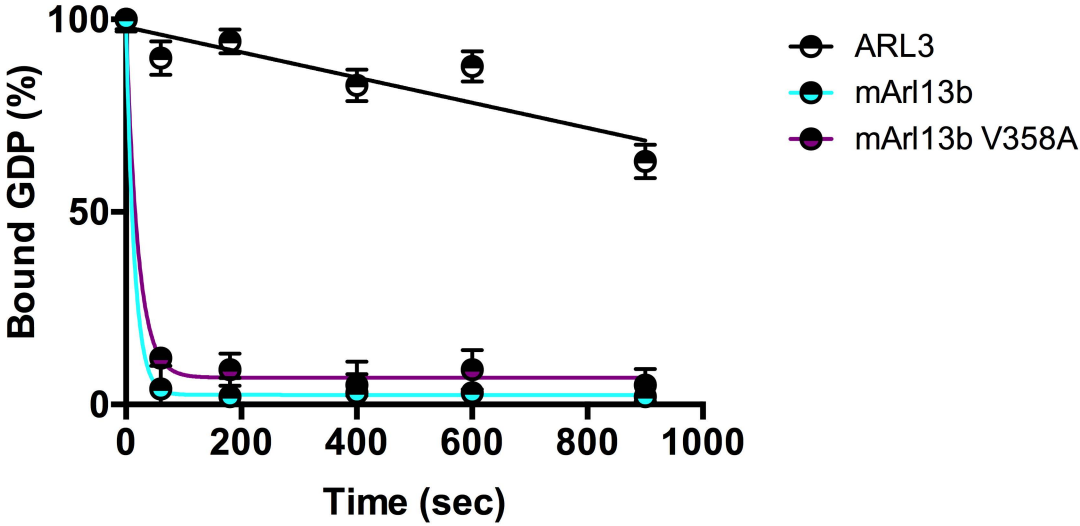
100
50
0
Bound GDP (%)
0
200
400
600
800
1000
Time (sec)
ARL3
mArl13b
mArl13b V358A

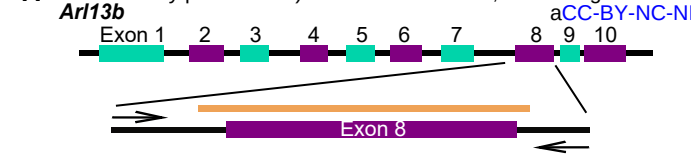

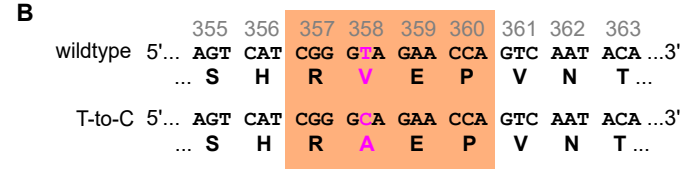

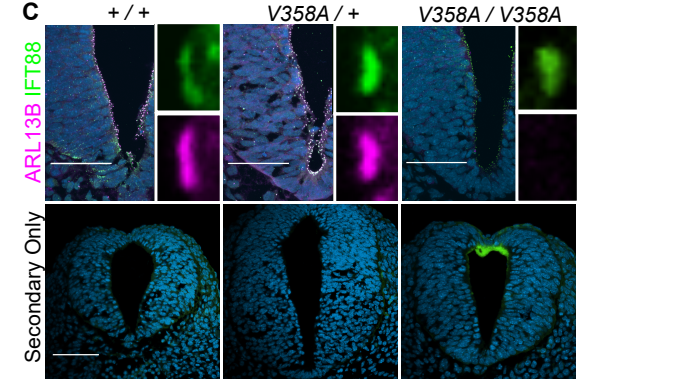

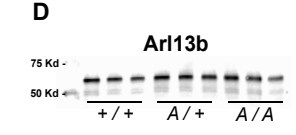

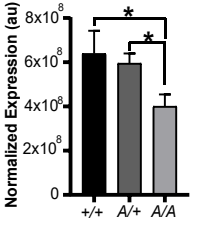

A

	PT	505	504	503	NM
Arl13b$^{+/+}$	204 (209)	223 (229)	147 (152)	223 (237)	55 (55)
Arl13b$^{V358A/+}$	154 (171)	147 (171)	148 (159)	134 (144)	90 (90)
Arl13b$^{V358A/V358A}$	0 (154)	0 (164)	0 (98)	0 (93)	0 (25)

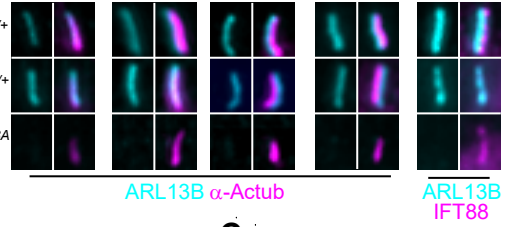

B

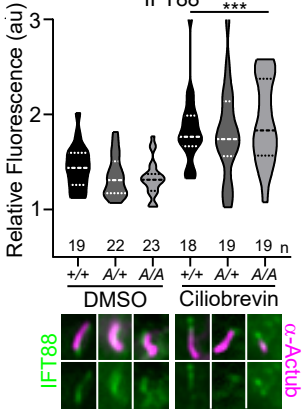

C

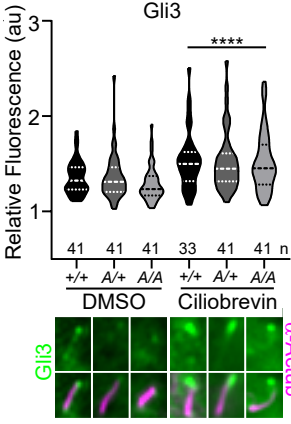

D

	DMSO	30μM CB
Arl13b$^{+/+}$	122 (129)	103 (112)
Arl13b$^{V358A/+}$	112 (126)	119 (129)
Arl13b$^{V358A/V358A}$	0 (131)	0 (118)

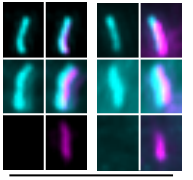

E

	DMSO	30μM CB
Arl13b$^{+/+}$	91 (94)	100 (113)
Arl13b$^{V358A/+}$	96 (107)	94 (99)
Arl13b$^{V358A/V358A}$	0 (77)	0 (111)

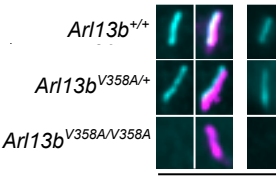

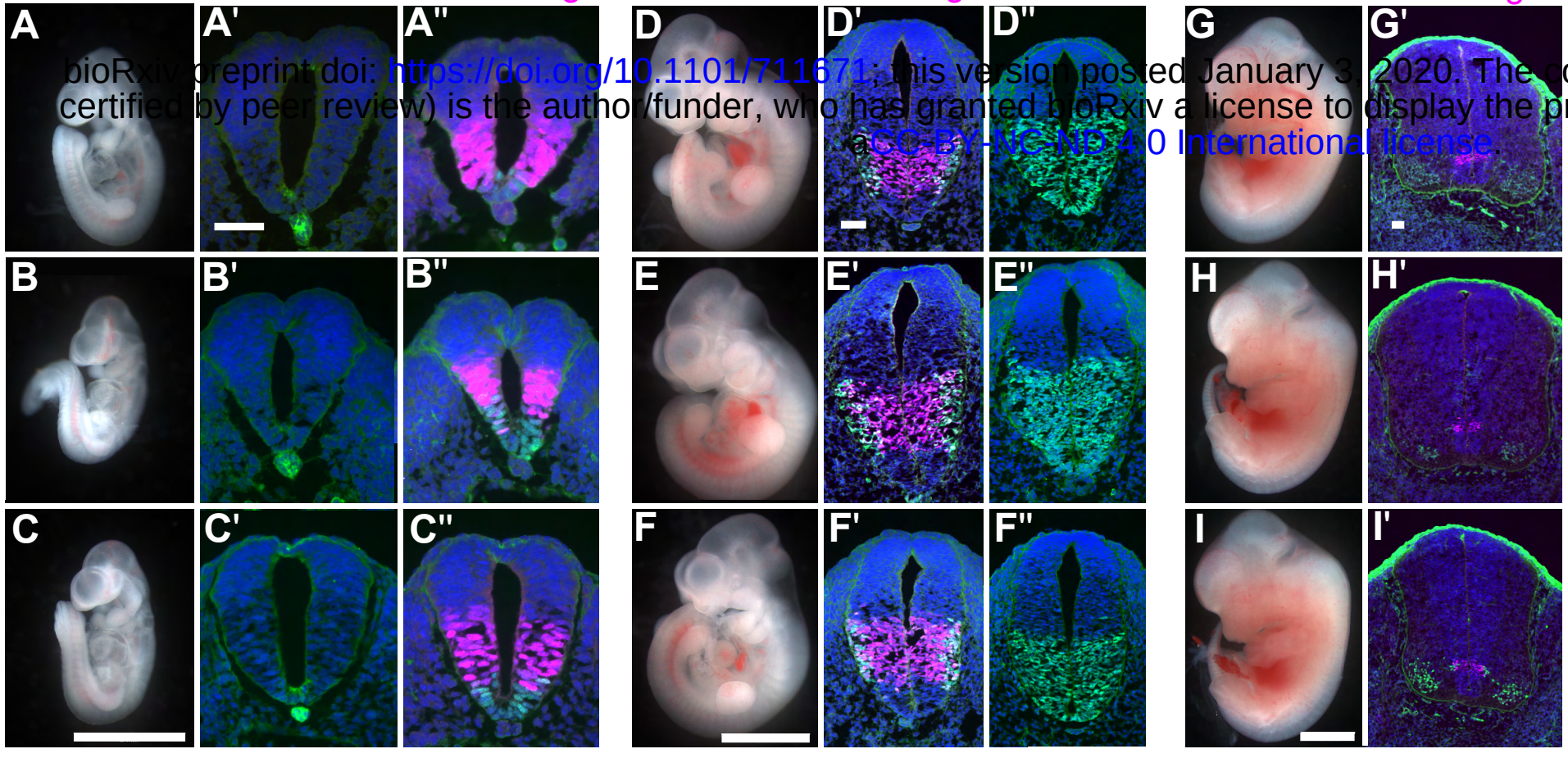

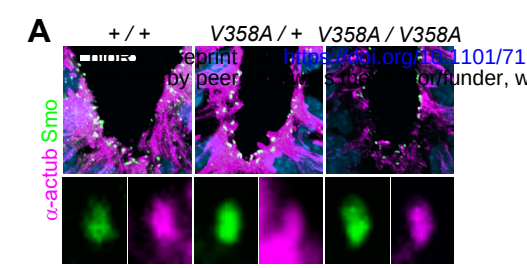

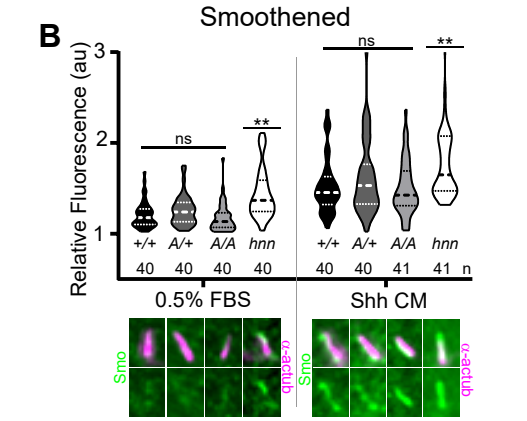

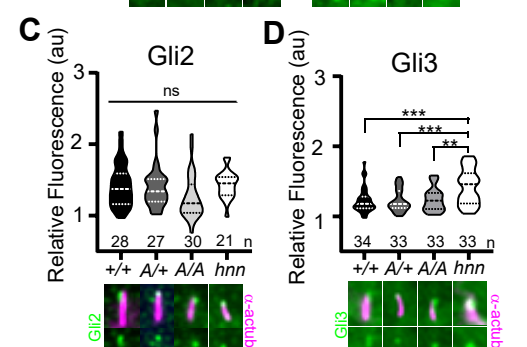

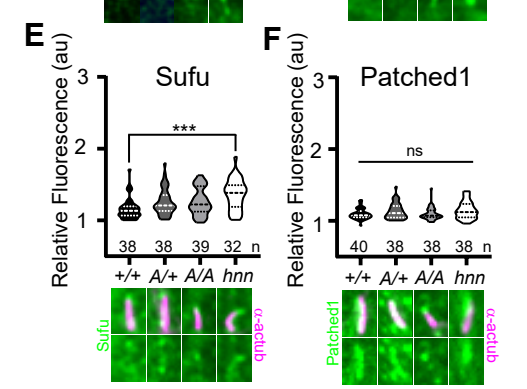

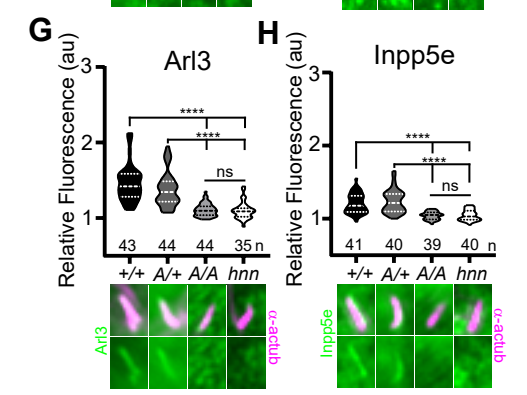

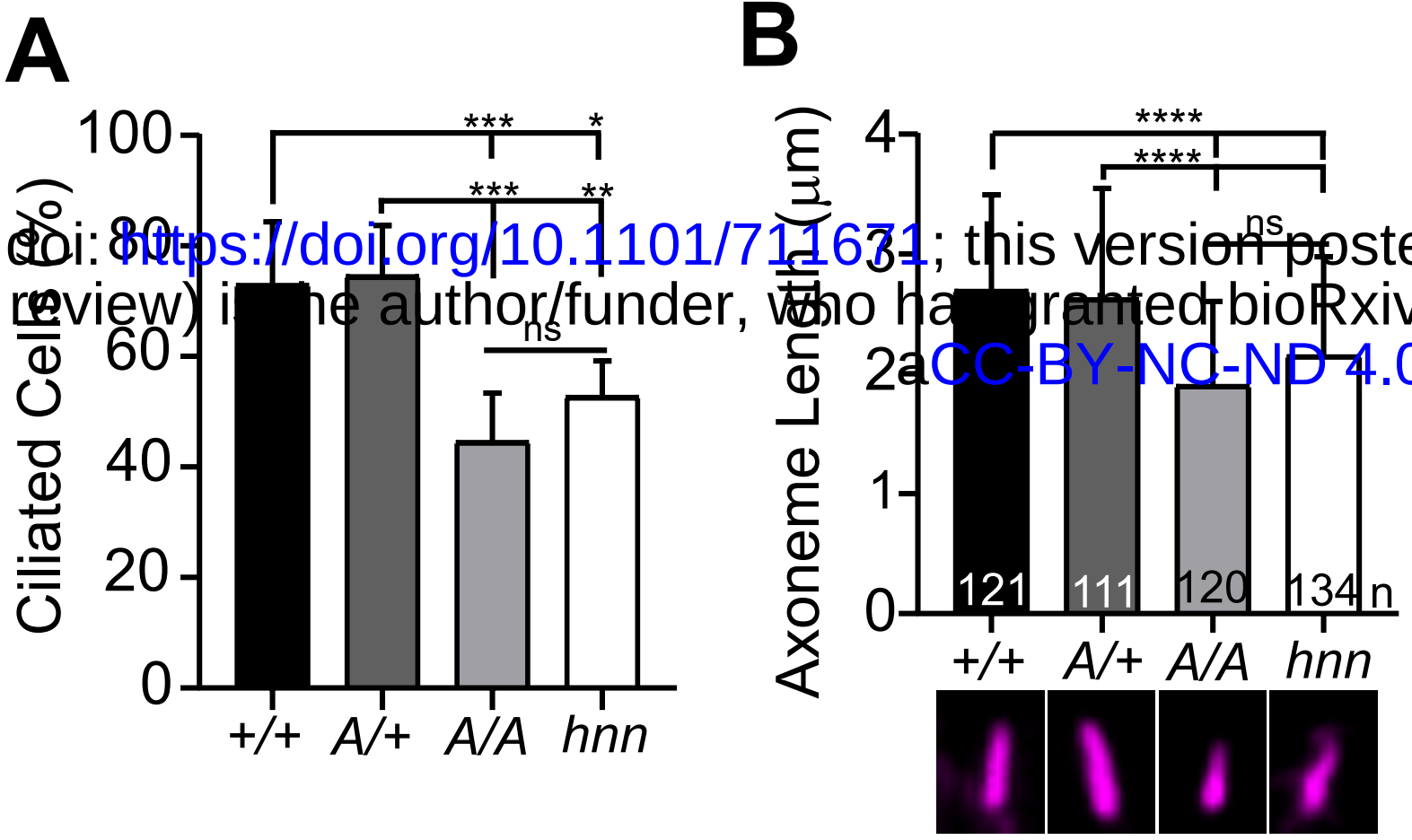

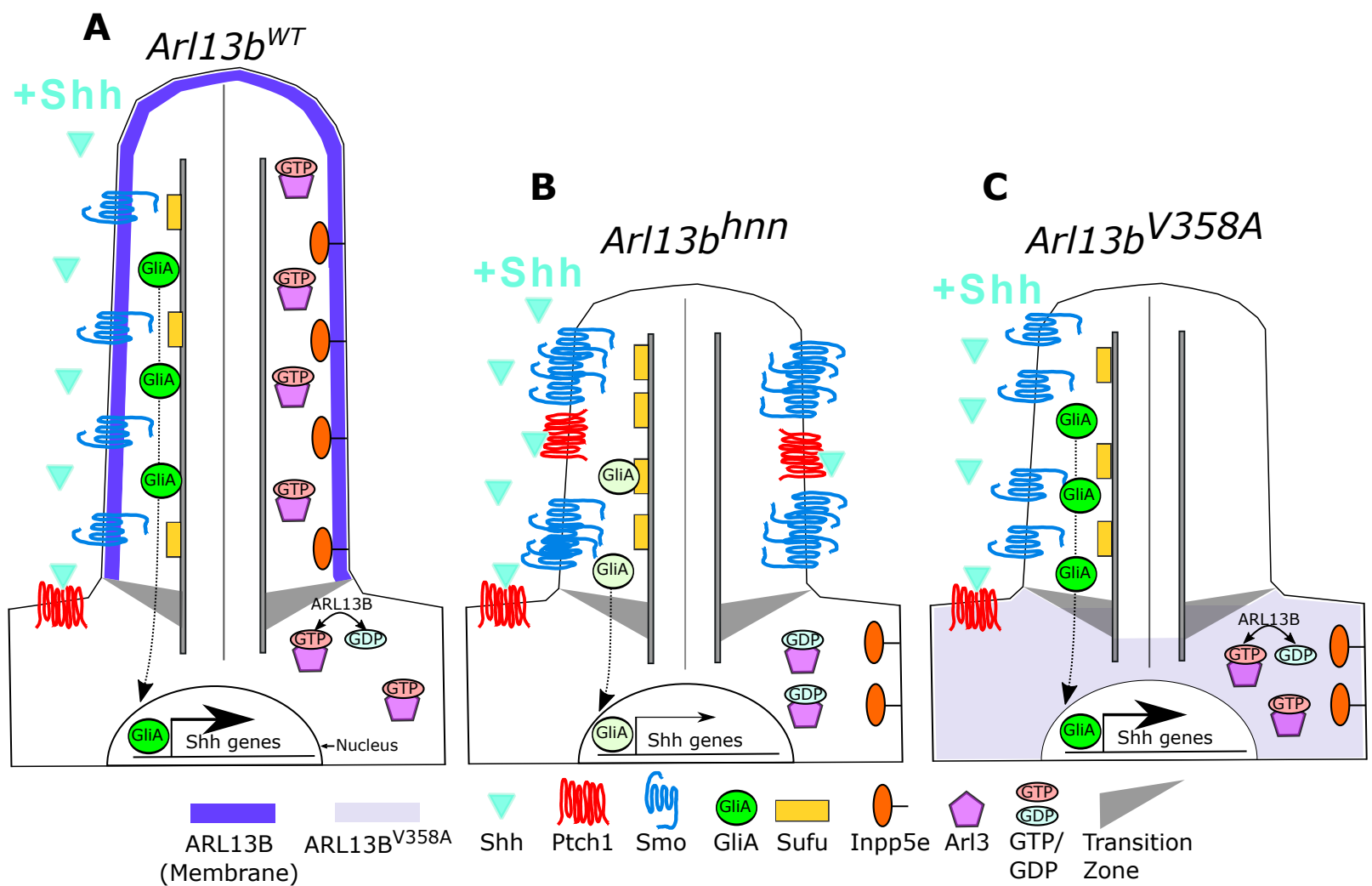
A
Arl13b^WT
+Shh
GTP
GliA
ARL13B
GDP
Shh genes
Nucleus
B
Arl13b^hnn
C
Arl13b^V358A
ARL13B (Membrane)
ARL13B^V358A
Shh
Ptch1
Smo
Sufu
Inpp5e
Arl3
GTP/ GDP
Transition Zone